ornl

ORNL/CON-154

OAK RIDGE
NATIONAL
LABORATORY

MARTIN MARIETTA

Nonlinear Analysis of Stirling Engine Thermodynamics

R. D. Banduric N. C. J. Chen

OPERATED BY
MARTIN MARIETTA ENERGY SYSTEMS, INC.
FOR THE UNITED STATES
DEPARTMENT OF ENERGY

Printed in the United States of America. Available from
National Technical Information Service
U.S. Department of Commerce
5285 Port Royal Road, Springfield, Virginia 22161
NTIS price codes—Printed Copy: A05; Microfiche A01

This report was prepared as an account of work sponsored by an agency of the United States Government. Neither the United States Government nor any agency thereof, nor any of their employees, makes any warranty, express or implied, or assumes any legal liability or responsibility for the accuracy, completeness, or usefulness of any information, apparatus, product, or process disclosed, or represents that its use would not infringe privately owned rights. Reference herein to any specific commercial product, process, or service by trade name, trademark, manufacturer, or otherwise, does not necessarily constitute or imply its endorsement, recommendation, or favoring by the United States Government or any agency thereof. The views and opinions of authors expressed herein do not necessarily state or reflect those of the United States Government or any agency thereof.

ORNL/CON-154

Engineering Technology Division

NONLINEAR ANALYSIS OF STIRLING ENGINE THERMODYNAMICS

R. D. Banduric N. C. J. Chen

Date Published: June 1984

Prepared by the
OAK RIDGE NATIONAL LABORATORY
Oak Ridge, Tennessee 37831
operated by
MARTIN MARIETTA ENERGY SYSTEMS, INC.
for the
U.S. DEPARTMENT OF ENERGY
under Contract No. DE-AC05-84OR21400

CONTENTS

Page

ACKNOWLEDGMENT v
ABSTRACT 1
1. INTRODUCTION 2
2. ENGINE LOSS ANALYSIS AND SOLUTION 4
2.1 Theoretical Formulation 4
2.2 Loss Mechanisms in the Engine Model 12
2.3 Method of Solution — Computer Application 14
3. ANALYSIS RESULTS — FOUR LOSS MECHANISMS 20
3.1 Adiabatic Loss 21
3.2 Transient Heat Transfer Loss 25
3.3 Pressure Drop Loss 28
3.4 Seal Leakage Loss 34
3.5 Coupled Loss Analysis 39
4. SUMMARY 43
REFERENCES 46
APPENDIX A. PROGRAM LISTING 47
APPENDIX B. VARIABLE LISTING 57
APPENDIX C. DERIVATIONS 61
APPENDIX D. RESULTS (TABULAR FORM) 67
APPENDIX E. RE-1000 DATA 73

ACKNOWLEDGMENT

The authors are indebted to F. P. Griffin and C. D. West of Oak Ridge National Laboratory Engineering Technology Division for their invaluable comments and constant encouragement.

NONLINEAR ANALYSIS OF STIRLING ENGINE THERMODYNAMICS

R. D. Banduric N. C. J. Chen

ABSTRACT

Numerical solutions to a simplified mathematical formulation for Stirling engine thermodynamics, including some major loss mechanisms and their interactions, are presented. The objective is to provide numerically accurate solutions to the nonlinear equations for verification of a simplified linear analysis recently developed at Oak Ridge National Laboratory. This was fully accomplished, and the results are quite interesting in their own right. At this stage, the formulation requires that the piston motions be specified; that is, it does not include the dynamics of free pistons. The equations of the formulation were numerically solved, with no further simplifications, using a standard IBM software package, called the Continous System Modeling Program, that basically involves numerical integration. The results were used to show the effects of four major loss mechanisms on the performance parameters of the RE-1000 free-piston Stirling engine. These losses are: adiabatic cylinder effects, transient heat transfer, pressure drop, and seal leakage. The performance parameters calculated were power output and efficiency. Some discussion of the results and a further analysis of this engine model are also presented.

The main accomplishments of this summer student project are:

1. the presentation of a computer solution of this third-order model formulation, with nonlinear effects considered, while the engine is operating with specified piston motions called the kinematic mode;
2. the demonstration of how this model will predict the trends of the effect of the four loss mechanisms on engine performance, while the engine is operating in the kinematic mode; and
3. the acquisition of numerically accurate solutions for later comparison with a newly developed linearized analysis.

1. INTRODUCTION

As part of the Department of Energy (DOE) Free-Piston Stirling/Rankine Hardware and Analytical Assessment Program, Oak Ridge National Laboratory (ORNL) is working on a thermodynamic and dynamic mathematical analysis of free-piston Stirling engines, which is intended to increase knowledge and understanding of these machines. A theoretical basis for such an understanding has already been conceived, and the first step in evaluating it is to estimate how well this theory will represent the effect of losses on engine performance while the engine is operating in the kinematic mode (i.e., with prescribed piston motions). The losses included in the model at present are: adiabatic, pressure drop, seal leakage, and transient heat transfer.

In the theory, the equations describing these effects are linearized, and to verify the validity of this simplification, the effect of nonlinear terms (i.e., nonlinear equation terms, nonlinear pressure drop correlations, etc.) must be evaluated. Such effects can be accounted for only by a numerical solution to the theoretical formulation. The main objective of this report is to present a numerical analysis, using existing IBM software, that will obtain a steady state solution to this engine model including the nonlinear terms. The results will then be used to illustrate the effect of the above losses, including their nonlinear effects, on engine power output and efficiency.

The mathematical model used here is a simplified "third-order" code (i.e., losses are coupled together) and is derived from the control volume approach. For this model, five control volumes were used, although three of them (the heater, regenerator, and cooler) are combined into a single, isothermal volume. In the expansion and compression control volumes, the gas is assumed to be well mixed. Thus, temperature and pressure gradient effects within each space were neglected. This approach leads to a description of the Stirling engine by a system of algebraic and ordinary (but nonlinear) differential equations.

The equations were solved for a given simulation by a numerical technique. The technique used involved integrating the differential equations forward in time. The integration was greatly simplified by using the IBM

Continuous System Modeling Program (CSMP III) that eliminated the need to develop a different computer code for the solution of the model equations. The CSMP package also has great flexibility in input algorithms. Thus, the numerical solution to the model's system of equations could be found rapidly and easily for many input conditions.

The effects of the losses on engine performance were illustrated by generating numerical solutions for various input values of the loss coefficients on a sample Stirling engine. These loss coefficients are constants that come from the mathematical model. In this way, all four of the losses (adiabatic, transient heat transfer, pressure drop, and seal leakage) can be simulated over a range of values. The effect of these losses are shown for both the decoupled (one loss only) and coupled (more than one loss) mode. The effects of nonlinear pressure drop correlations and high engine compression ratios that are expected to increase the importance of nonlinearities were also analyzed.

The engine simulated in this report is basically similar to the RE-1000 Free-Piston Stirling Engine (manufactured by Sunpower Inc.). Although the piston motions are prescribed, the values are based on experimental measurements made at National Aeronautics and Space Administration—Lewis Research Center. This engine is basically a low compression ratio (about 1.3 :1) machine, with a nominal power output of 1000 W. More data on the engine are given in Appendix E.

The remainder of this report is organized as follows. Section 2 contains the mathematical formulation and description of the developed computer program based on CSMP, as well as a description of the four loss mechanisms. Section 3 contains the results of the loss mechanism analysis that includes: the effect of the adiabatic loss for various engine compression ratios (Sect. 3.1), the effect of the transient heat transfer loss for different values of the heat transfer coefficient (Sect. 3.2), the effect of pressure drop for both linear and nonlinear correlations (Sect. 3.3), the effect of seal leakage for both linear and nonlinear correlations (Sect. 3.4), and the effect of coupling the pressure drop and seal leakage losses together (Sect. 3.5). Finally, Sect. 4 will summarize the results and present conclusions and recommendations.

2. ENGINE LOSS ANALYSIS AND SOLUTION

This section will provide the background necessary for simulating the effects of the losses on engine performance. The theoretical formulation, a detailed analysis of the loss mechanisms and how they are included in the model, and a numerical solution to the equations are discussed.

2.1 Theoretical Formulation

The theoretical formulation for the free-piston Stirling engine was derived from the control volume approach. For this formulation, five control volumes were used: expansion and compression spaces, heater, cooler, and regenerator. However, the three heat exchanger components are considered to behave isothermally, and so their effects can be combined into a single "dead" volume (Fig. 1). Within each working space (expansion and compression), the gas is considered to be at a uniform temperature and pressure. In addition, the following other assumptions were made.

1. The dead space is isothermal.
2. The dead space pressure is uniform at any time.
3. The piston variations are sinusoidal.
4. Gas inertia effects are negligible.
5. Engine wall temperatures are constant with time.

With these assumptions, a system of both algebraic and ordinary differential equations can be written from the above model to describe the steady state operation of the engine. The derivation of these equations follows.

The algebraic relations will be derived first. The first relation describes the volume variations. The piston variations were assumed sinusoidal. Thus,

$$X_p = X_{pamp} \sin \omega t \ , \tag{1}$$

$$X_d = X_{damp} \sin(\omega t + B) \ . \tag{2}$$

ORNL–DWG 83–5936A ETD

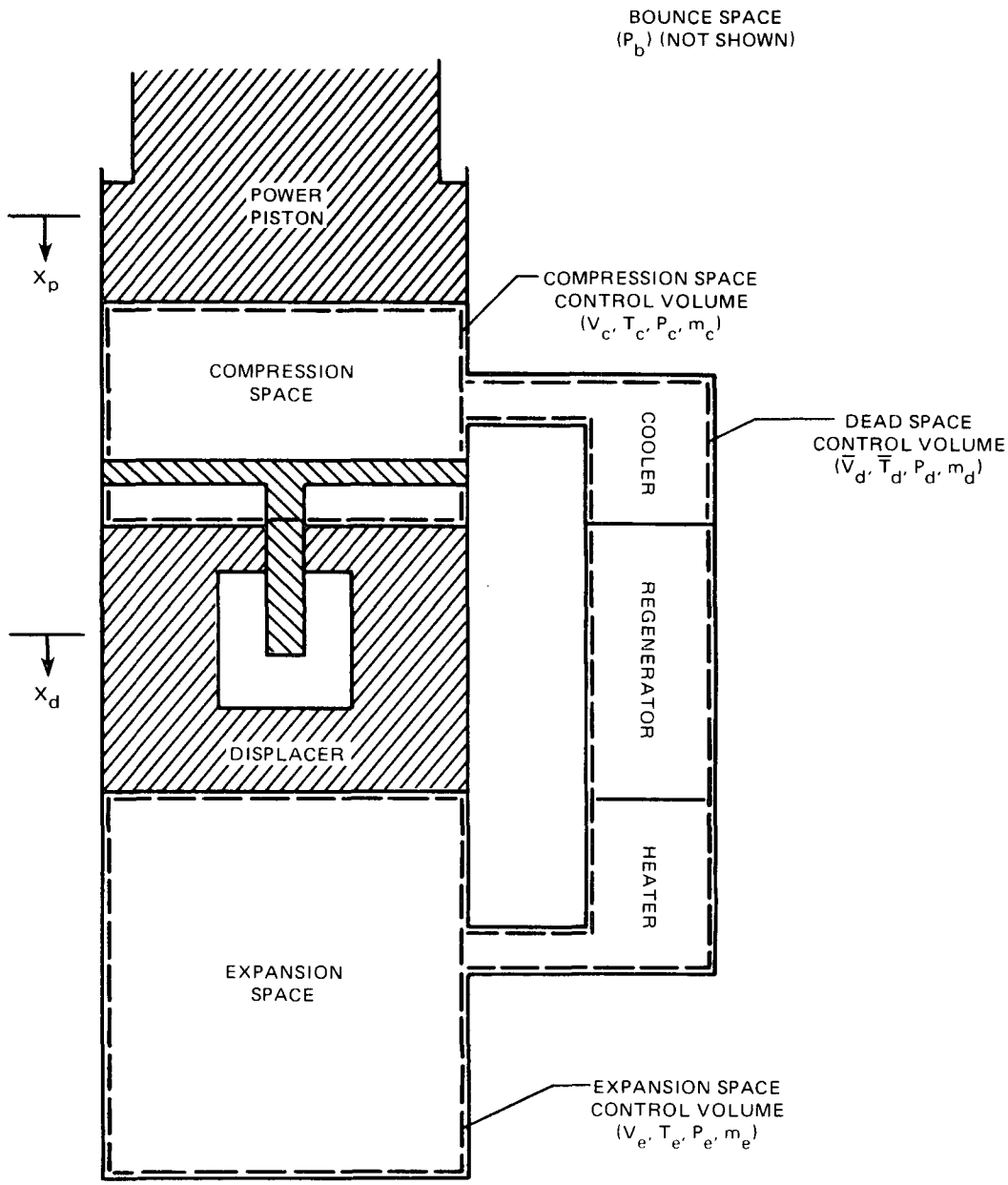

Fig. 1. RE-1000 engine schematic.

From Fig. 1, the volume variations are

$$V_e = \overline{V}_e - A_d X_d , \tag{3}$$

$$V_c = \overline{V}_c + (A_d - A_r) X_d - A_p X_p . \tag{4}$$

Substituting Eq. (2) into Eq. (3) and Eqs. (1) and (2) into Eq. (4) and simplifying, the volume variations are

$$V_e = \overline{V}_e - V_{eamp} \sin(\omega t + B_1) \ , \tag{5}$$

$$V_c = \overline{V}_c + V_{camp} \sin(\omega t + B_2) \ , \tag{6}$$

where

$\overline{V}_e$ = average expansion space volume,
$\overline{V}_c$ = average compression space volume,
ω = engine frequency (rad/s),
B = phase angle between displacer and power piston (rad),
X_{damp} = displacer amplitude,
X_{pamp} = piston amplitude,
A_d = displacer cross-sectional area,
A_p = piston cross-sectional area,
A_r = displacer rod cross-sectional area,
$B_1 = B$,
$B_2 = \tan^{-1} \{(A_d - A_r) X_{damp} \sin B / [(A_d - A_r) X_{damp} \cos B - A_p X_{pamp}]\}$,
$V_{eamp} = A_d X_{damp}$,
$V_{camp} = \{[(A_d - A_r) X_{damp} \sin B]^2 + [(A_d - A_r) X_{damp} \cos B - A_p X_{pamp}]^2\}^{1/2}$.

All quantities in Eqs. (5) and (6) are known from engine specifications. Thus, the volume variations are prescribed, sinusoidal functions of time.

Three other relations come from the equation of state for each space. For this particular case, the perfect gas law is a good approximation. Thus,

$$\frac{P_e V_e}{m_e T_e} = R \ , \tag{7}$$

$$\frac{P_c V_c}{m_c T_c} = R \ , \tag{8}$$

$$\frac{P_d}{m_d} = \frac{R\,\overline{T}_d}{\overline{V}_d}\,, \tag{9}$$

where

P_e, P_d, P_c = pressure in each space,
m_e, m_d, m_c = mass of working gas in each space,
T_e, $\overline{T}_d$, T_c = temperature of working gas in each space (constant for dead space),
V_e, $\overline{V}_d$, V_c = volume of each space (constant for dead space).

Note that the volume and temperature of the dead space are constant with time. $\overline{V}_d$ comes from engine specifications. However, $\overline{T}_d$ must come from some kind of spatial average for the temperature distribution that actually exists in that space. The following formula gives a good approximation of this average temperature.

$$\overline{T}_d = \overline{V}_d \Bigg/ \left(\frac{V_{dh}}{T_{heat}} + \frac{V_{dc}}{T_{cool}} + \frac{V_{dr}}{T_{reg}} \right)\,, \tag{10}$$

where

T_{heat}, V_{dh} = heater temperature and volume,
T_{cool}, V_{dc} = cooler temperature and volume,
T_{reg}, V_{dr} = regenerator effective temperature and volume.

Equation (10) is derived in Appendix C.

Mass conservation gives the final algebraic relation. By applying the conservation of mass,

$$m_w = m_e + m_c + m_d\,, \tag{11}$$

where m_w = total mass of working gas.

The rest of the relations for this model are described by ordinary differential equations. Two equations come from a first-law analysis of the working spaces (expansion and compression). Note that because of the uniform pressure and temperature assumptions, these spaces are uniform

state, uniform flow, and deformable control volumes. The energy equation for such a control volume is given by[1]

$$\begin{array}{ccccccc} du & + & PdV & = & Q_1 & + & Q_2 \\ \begin{pmatrix}\text{internal}\\ \text{energy}\\ \text{increase}\end{pmatrix} & + & \begin{pmatrix}\text{work}\\ \text{output}\end{pmatrix} & = & \begin{pmatrix}\text{heat from}\\ \text{enthalpy}\\ \text{flux}\end{pmatrix} & + & \begin{pmatrix}\text{heat from wall}\\ \text{heat transfer}\end{pmatrix} \end{array} . \tag{12}$$

The above quantities are shown for the expansion space in Fig. 2. From Eq. (12) and Fig. 2,

$$\frac{d}{dt}(m_e c_v T_e) + P_e \frac{dV_e}{dt} = \frac{dm_e}{dt} c_p T_{fe} + h_e \bar{A}_{se} (\bar{T}_{we} - T_e) . \tag{13}$$

Simplifying and rearranging,

$$\frac{dT_e}{dt} = -\frac{T_e}{m_e}\frac{dm_e}{dt} - \frac{(\gamma - 1) T_e}{V_e}\frac{dV_e}{dt} + \frac{\gamma}{m_e}\frac{dm_e}{dt} T_{fe} + \frac{h_e \bar{A}_{se}}{m_e c_v}(\bar{T}_{we} - T_e) , \tag{14}$$

where

γ = ratio of specific heats,

h_e = heat transfer coefficient in the expansion space,

$\bar{A}_{se}$ = average wall surface area in the expansion space,

$\bar{T}_{we}$ = average wall temperatures in the expansion space,

$$T_{fe} = \begin{cases} T_e & \text{if } dm_e/dt < 0 \\ T_{heat} & \text{if } dm_e/dt > 0 \end{cases} .$$

T's, V's and m's are defined as before. Similarly, for the compression space (Fig. 2),

$$\frac{dT_c}{dt} = -\frac{T_c}{m_c}\frac{dm_c}{dt} - \frac{(\gamma - 1)T_c}{V_c}\frac{dV_c}{dt} + \frac{\gamma}{m_c}\frac{dm_c}{dt} T_{fc} + \frac{h_c \bar{A}_{sc}}{m_c c_v}(\bar{T}_{wc} - T_c) , \tag{15}$$

ORNL–DWG 83–5937 ETD

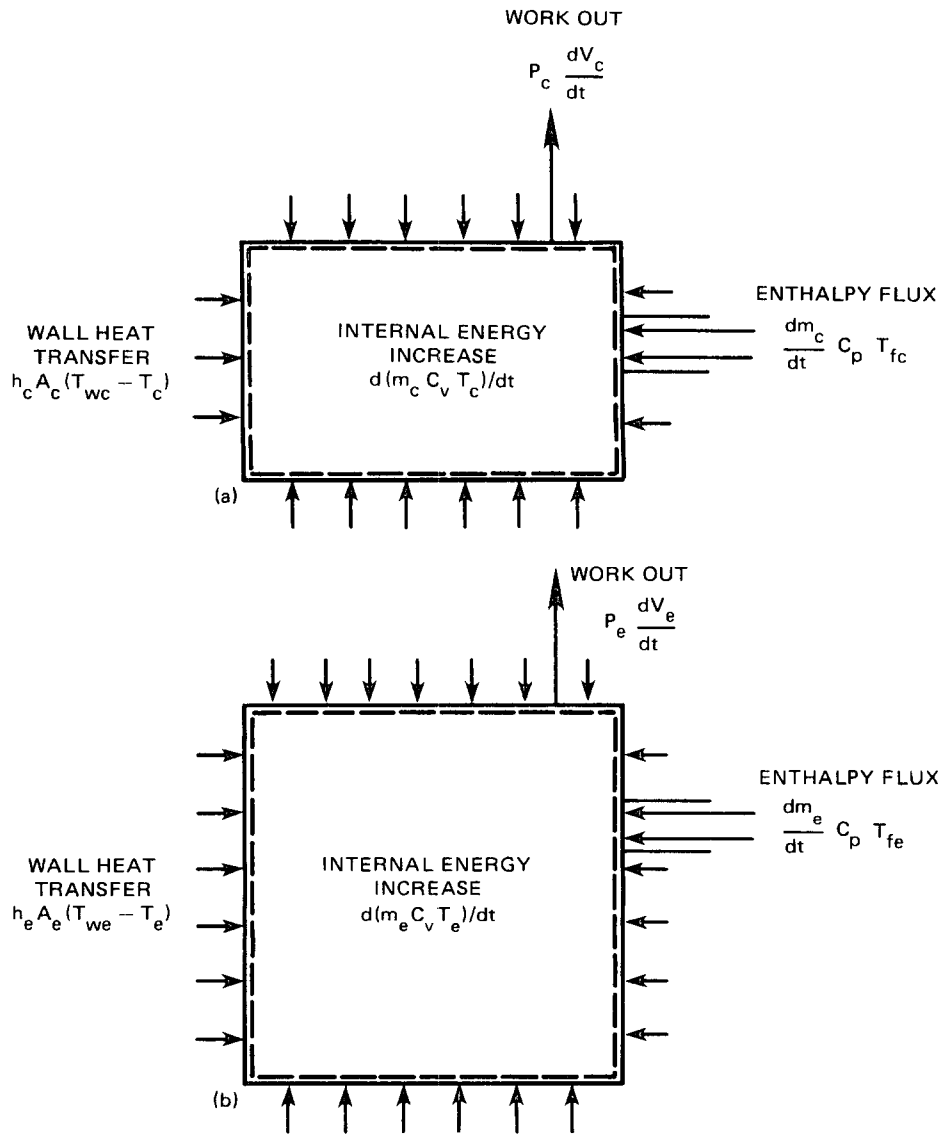

Fig. 2. Control volume energy balance.

where

$$T_{fc} = \begin{cases} T_{cool} & \text{if } dm_c/dt > 0 \\ T_c & \text{if } dm_c/dt < 0 \end{cases} .$$

T's, V's, m's, h's etc. are all defined as before. Note that there is a temperature discontinuity, which, in turn, causes an enthalpy flux

discontinuity. This occurs because, in our formulation, the gas enters the space at the temperature of the adjacent heat exchanger (T_{heat} for expansion space, T_{cool} for compression space), but leaves at the working space temperature (T_e for expansion space, T_c for compression space).

Three last differential equations come from pressure drop relations. Here, the mass flow rate through an engine passage is related to the pressure drop across the passage. In this model, three such passages exist: (1) gas flow from dead volume to compression space, (2) gas flow from dead volume to expansion space, and (3) leak from compression space to bounce space.

Many correlations exist for this relation. For simplicity, the power law will be used in this formulation:

$$\frac{dm}{dt} = k\ (\Delta P)^n\ . \tag{16}$$

Applying Eq. (16) to each passage,

$$\frac{dm_e}{dt} = k_{de}\ (P_d - P_e)^{n_{de}}\ , \tag{17}$$

$$\frac{dm_c}{dt} = k_{dc}\ (P_d - P_c)^{n_{dc}} + k_{bc}\ (P_b - P_c)^{n_{bc}}\ , \tag{18}$$

$$\frac{dm_w}{dt} = k_{bc}\ (P_b - P_c)^{n_{bc}}\ , \tag{19}$$

where

k = flow coefficients,

n = exponents,

P_b = bounce space pressure.

The values of these constants depend on the flow geometry and characteristics and are best found experimentally.

Finally, for engine performance evaluation, the engine power output and efficiency must be expressed. These quantities are found by evaluating the expressions for work output for a deformable control volume over a cycle. This expression is[2]

$$W_{out} = \oint P dV \ . \tag{20}$$

This expression was evaluated for each space over a complete cycle. The quantities were then multiplied by the frequency to get the power output. The resulting integrals are

$$\begin{aligned} Q_{in} &= f\oint P_e dV_e \text{ (expansion space)} \ , \\ Q_{out} &= -f\oint P_c dV_c \text{ (compression space)} \ . \end{aligned} \tag{21}$$

Thus, the work output is

$$W_{out} = f(\oint P_e dV_e + \oint P_c dV_c) \ . \tag{22}$$

Finally, an engine efficiency must be defined. Our definition is

$$\text{Eff} = \frac{\text{work output}}{\text{heat input}} \ .$$

For this engine, the heat input is the heat flow into the expansion space. Thus,

$$\text{Eff} = \frac{W_{out}}{Q_{in}} = 1 + \frac{\oint P_c f V_c}{\oint P_e dV_e} \ . \tag{23}$$

The steady state operation and the main engine performance indicators of a Stirling engine are given by the solution to Eqs. (21)—(23). The equations demonstrate some inherent losses in the engine, which will be discussed in the next section.

2.2 Loss Mechanisms in the Engine Model

This engine model can simulate four different losses: (1) adiabatic; (2) transient heat transfer; (3) pressure drop; and (4) seal leakage. Each loss will be discussed in detail, and the coupling effect of some of them will be considered.

The adiabatic loss results from the temperature differences between the dead space and the working spaces (expansion and compression). These temperature differences lead to losses because heat is transferred across them. The heat transfer is due to the enthalpy flux term in the energy equation. The temperature differences occur because the dead space is fairly isothermal, while the gas in the working spaces fluctuates widely in temperature. These temperature swings can be moderated by heat transfer from and to the cylinder walls. In fact, infinite heat transfer (instantaneous heat transfer) would theoretically make the gas in the working spaces behave isothermally.

The adiabatic loss is represented in this model by the temperature discontinuity in the energy equation. This term, from the expansion energy equation [Eq. (13)], is

$$c_p \frac{dm_e}{dt} T_{fe} = \begin{cases} c_p \dfrac{dm_e}{dt} T_{heat} & \text{if } \dfrac{dm_e}{dt} > 0 \\ c_p \dfrac{dm_e}{dt} T_e & \text{if } \dfrac{dm_e}{dt} < 0 \end{cases} .$$

A similar expression is found for the compression space. This loss is inherent in the equations — as it should be — and will increase as the temperature fluctuations in both working spaces increase. This phenomenon will be further explored in Sect. 3.1.

The transient heat transfer loss comes from the heat transfer due to the temperature differences between the working gas and the cylinder walls. As stated before, the gas temperatures in the working spaces tend to fluctuate, but the cylinder walls, having a higher heat capacity, tend

to remain at a constant temperature. Heat transfer between the gas and the engine wall occurs over a fluctuating and fairly substantial temperature difference. This, like the adiabatic loss, produces a loss accounted for by the second law of thermodynamics. In the model, this loss is represented in the heat transfer term of the energy equation by [from the expansion space energy equation, Eq. (13)]

$$h_e \bar{A}_{se} (\bar{T}_{we} - T_e) .$$

There is a similar term in the compression space energy equation. Note that the controlling variables in this expression are both h_e and T_e ($\bar{T}_{we}$ is assumed constant). Also note that the term is zero for an adiabatic cylinder ($h_e = 0$) and for an isothermal cylinder ($\bar{T}_{we} = T_e$). It follows that there is a worst case (i.e., maximum transient heat transfer loss) for a certain value of h_e between zero and infinity. This phenomenon will be explored further in Sect. 3.2.

The pressure drop loss is due to the working gas pressure drop as it flows through the heat exchanger components; more basically, the working gas loses power due to friction as it flows through these components. As a result, some engine input energy must go to overcoming the pressure drop.

The seal leakage loss is similar to the pressure drop loss in that the working fluid loses power due to friction, but it is caused by the fluid leak from the working space. Such a leak causes the working gas to flow back and forth between the compression and bounce spaces. There is a loss because energy must be spent to cause the fluid to flow between the two spaces.

Both the pressure drop and seal leakage losses are modeled the same way in our engine. The pressure drop loss is represented by Eqs. (17) and (18)

$$\frac{dm_e}{dt} = k_{de} (P_d - P_e)^{n_{de}} , \tag{17}$$

$$\frac{dm_c}{dt} = k_{dc} (P_d - P_c)^{n_{dc}} + k_{bc} (P_b - P_c)^{n_{bc}} . \tag{18}$$

Mass leakage is modeled by Eq. (19)

$$\frac{dm_w}{dt} = k_{bc} \left(P_b - P_c\right)^{n_{bc}} . \tag{19}$$

These correlations will approximate these flow losses. Note that even though the leakage and pressure drop losses are modeled in the same way, they are not the same physical process. For example, a situation with no leakage loss is modeled with $k_{bc} = 0$ (m_w = constant), while one with no pressure drop loss is modeled with k_{de}, $k_{dc} = \infty$ ($P_d - P_e = 0$ and $P_d - P_c = 0$ for any finite mass flow rate). The effects of the two losses on engine performance are also different. These differences will be explored in Sects. 3.3 and 3.4.

Pressure drop and seal leakage losses can be modeled individually or together. Since this is a third-order type of code, it is possible to estimate the effect of coupling of losses on engine performance. In other words, we may address the question, "Can two losses treated individually (decoupled mode) be simply added together to show the effects of both losses acting together (coupled or third-order mode)?" Such a question is important, because if the losses are essentially decoupled, second-order analyses would be accurate, which would lead to lower computing costs and also to a simpler representation of these losses. This type of analysis will be discussed in Sect. 3.5.

In conclusion, the pressure drop and leakage losses can be simulated by this model for many situations. To demonstrate these losses, a steady state solution to the equations must be found for various input conditions. This can be done by numerical integration on a computer. This integration solution is explored in the next section.

2.3 Method of Solution — Computer Application

Part of the objective of this analysis is to simulate the losses in this model, taking all nonlinear terms into account. This means finding the solution to the previously derived system of nonlinear differential equations and algebraic relations without further simplification, which

can be accomplished only by a numerical technique. A numerical solution making use of the IBM CSMP subroutine was developed for this engine model and is described in this section.

Using the CSMP software greatly simplified the programming, because the CSMP provided subroutines that could do the necessary numerical integrations at each time step. Also, this CSMP subroutine had several input switch statements that made modeling of the temperature discontinuity easy; thus, the programming of this program mainly involved inputting the proper equations in the correct order.

CSMP does place certain restrictions on the equations that could be inputed:

1. Large values of the flow coefficients and heat transfer coefficient could not be used because of numerical stability problems.
2. All derivative terms had to be inputted explicitly in terms of non-derivatives.
3. All derivatives must be first order.

As a result of these restrictions, two programs had to be written. One is used when there is pressure drop in the simulation (program A); the other is used when there is no pressure drop (program B).

Program A was, perhaps surprisingly, the simpler of the two, because all derivatives in the differential equations are already written in explicit forms.

$$\frac{dV_e}{dt} = \frac{d}{dt}(V_e) = -\omega\, V_{eamp} \quad \cos(\omega t + B_1) ,$$

$$\frac{dV_c}{dt} = \frac{d}{dt}(V_c) = \omega\, V_{camp} \quad \cos(\omega t + B_2) ,$$

$$\frac{dm_e}{dt} = k_{de}\,(P_d - P_e)^{n_{de}} ,$$

$$\frac{dm_c}{dt} = k_{dc}\,(P_d - P_c)^{n_{dc}} + k_{bc}\,(P_b - P_c)^{n_{bc}} ,$$

$$\frac{dm_w}{dt} = k_{bc} \left(P_b - P_c\right)^{n_{bc}} ,$$

$$\frac{dT_e}{dt} = \frac{-T_e}{m_e} \frac{dm_e}{dt} - \frac{(\gamma - 1)\, T_e}{V_e} \frac{dV_e}{dt} + \frac{\gamma}{m_e} \frac{dm_e}{dt} T_{fe} + \frac{h_e \bar{A}_{se}}{m_e c_v} \left(\bar{T}_{we} - T_e\right) ,$$

$$\frac{dT_c}{dt} = \frac{-T_c}{m_c} \frac{dm_c}{dt} - \frac{(\gamma - 1)\, T_c}{V_c} \frac{dV_c}{dt} + \frac{\gamma}{m_c} \frac{dm_c}{dt} T_{fc} + \frac{h_c \bar{A}_{sc}}{m_c c_v} \left(\bar{T}_{wc} - T_c\right) .$$

Note that all derivatives are in terms of nonderivative terms. Thus, the equations can be merely inputted in a logical order.

Some other programming was required for program A. A "switch" was used to represent the temperature discontinuity. Some FORTRAN logic using subscripted variables was also used to take the limits on the work integrals. This programming will not be discussed here; a listing of program A is given in Appendix A.1.

Program B was somewhat more complicated, but necessary to simulate no pressure drop cases. To simulate no pressure drop with program A, the flow coefficient must be set to a large number (theoretically, infinity), and such an input caused numerical stability problems. The equations must be manipulated prior to computation to ensure numerical stability. This manipulation involved eliminating the pressure drop relations by realizing that the pressure is uniform in the working gas at all times. Then, a combination of the equations of state [Eqs. (7) to (9)] and the energy equations [Eqs. (14) and (15)] will result in stable relations for CSMP. This derivation is given in Appendix C as Eq. (C.9). The result of the manipulation is given below.

$$m_e = \frac{m_w V_e / T_e}{V_{red}} , \tag{24}$$

$$m_c = \frac{m_w V_c / T_c}{V_{red}} , \tag{25}$$

$$m_d = \frac{m_w \, \overline{V}_d / \overline{T}_d}{V_{red}} , \tag{26}$$

$$\begin{bmatrix} C_{11} & C_{12} \\ C_{21} & C_{22} \end{bmatrix} \begin{bmatrix} \frac{dTe}{dt} \\ \frac{dTc}{dt} \end{bmatrix} = \begin{bmatrix} F_1(t) \\ F_2(t) \end{bmatrix} , \tag{27}$$

where

$$V_{red} = \frac{V_e}{T_e} + \frac{V_c}{T_c} + \frac{\overline{V}_d}{\overline{T}_d} ,$$

$$C_{11} = 1 + (T_e - \gamma T_{fe}) \left(\frac{1}{-T_e} + \frac{V_e}{V_{red}} \frac{1}{T_e^{\,2}} \right) ,$$

$$C_{12} = (T_e - \gamma T_{fe}) \frac{V_c}{T_c^2 \, V_{red}} ,$$

$$C_{21} = (T_c - \gamma T_{fc}) \frac{V_e}{T_e^{\,2} \, V_{red}} ,$$

$$C_{22} = 1 + (T_c - \gamma T_{fc}) \left(- \frac{1}{T_c} + \frac{V_c}{T_c^{\,2} \, V_{red}} \right) ,$$

$$F_1 = -\left[(\gamma - 1)T_e + (T_e - \gamma T_{fe})\left(1 - \frac{V_e}{T_e\, V_{red}}\right)\right]\frac{1}{V_e}\frac{dVe}{dt}$$

$$+ (T_e - \gamma T_{fe})\frac{V_c}{T_c\, V_{red}}\frac{1}{V_c}\frac{dVc}{dt} + \frac{dm_w}{dt}\frac{1}{m_w}(\gamma T_{fe} - T_e)$$

$$+ \frac{h_e\, \overline{A}_{se}}{c_v\, m_e}(\overline{T}_{we} - T_e) ,$$

$$F_2 = (T_c - \gamma T_{fc})\frac{V_e}{T_e\, V_{red}}\frac{1}{V_e}\frac{dV_e}{dt} + \frac{dm_w}{dt}\frac{1}{m_w}(\gamma T_{fc} - T_c)$$

$$- \left[(\gamma - 1)T_c + (T_c - \gamma T_{fc})\left(1 - \frac{V_c}{T_c V_{red}}\right)\right]\frac{1}{V_c}\frac{dV_c}{dt}$$

$$+ \frac{h_c\, \overline{A}_{sc}}{c_v\, m_c}(\overline{T}_{wc} - T_c) .$$

Equation (27) gives two equations for two unknowns (dT_e/dt, dT_c/dt) that can be solved explicitly by using Cramers rule. Thus,

$$\frac{dTe}{dt} = \frac{\begin{bmatrix} F_1 & C_{12} \\ F_2 & C_{22} \end{bmatrix}}{\begin{bmatrix} C_{11} & C_{12} \\ C_{21} & C_{22} \end{bmatrix}} , \tag{28}$$

$$\frac{dTc}{dt} = \frac{\begin{bmatrix} C_{11} & F_1 \\ C_{21} & F_2 \end{bmatrix}}{\begin{bmatrix} C_{11} & C_{12} \\ C_{21} & C_{22} \end{bmatrix}} . \tag{29}$$

Note that the number of differential relations is reduced from five to three (two pressure drop relations being eliminated). This is physically

reasonable because three of the unknowns (P_e, P_c, P_d) are replaced by a single unknown (P_w). Also note that the temperatures are now coupled together by rather complicated expressions. This coupling indicates how truly complicated the analysis is even for this extremely simple model.

One other piece of programming was required for program B. For this analysis, the sign of dm/dt is required to calculate the temperature discontinuity. To evaluate this in program B, the following approximation was used:

$$\frac{dm}{dt} = \frac{m - m_o}{t_{step}} , \tag{30}$$

where

m = current gas mass,

m_o = old gas mass (previous time step),

t_{step} = time step.

This expression is a good approximation of this derivative and is almost exactly accurate when only the sign (positive or negative) is needed. The programming techniques used to evaluate work integrals and temperature discontinuities are the same as before. This program is also given in Appendix A.2.

One other stability problem occurred in both programs. This problem occurred when isothermal conditions were simulated by using high heat transfer coefficients. Isothermal conditions were instead simulated by specifying the unit-specific heat ratio ($\gamma = 1$). With such an input, the temperature of the gas within the cylinders remained constant throughout the simulation as would be the case for isothermal behavior.

In conclusion, the program can be used to analyze the mathematical model for many different input conditions. One of its uses is to simulate four major loss mechanisms in a Stirling engine (i.e., adiabatic, transient heat transfer, pressure drop, and seal leakage) individually or simultaneously. How these losses affect engine performance and each other can be shown by the model through solutions obtained with the programs described here. This will be demonstrated in Sect. 3.

3. ANALYSIS RESULTS — FOUR LOSS MECHANISMS

This section will explore the four loss mechanisms by solving the mathematical formulation of the engine with the CSMP computer package. More specifically, the simulation will show the effect of:

1. the adiabatic loss for various engine compression ratios (Sect. 3.1);
2. the adiabatic loss and transient heat transfer loss together for various values of the cylinder heat transfer coefficient (Sect. 3.2);
3. the pressure drop for both linear and nonlinear pressure drop correlations (Sect. 3.3);
4. seal leakage for both linear and nonlinear leakage correlations (Sect. 3.4); and
5. the coupling between the seal leakage and pressure drop losses (Sect. 3.5).

These losses will be demonstrated using data typical of the RE-1000 free-piston Stirling engine, but with specified piston motions. The main operating characteristics of the RE-1000 free-piston Stirling engine are

1. heater temperature = 900 K;
2. cooler temperature = 300 K;
3. engine frequency = 30 Hz;
4. displacer to power piston phase angle = 45°;
5. working fluid = helium; and
6. compression ratio = 1.30:1.

These six characteristics will be used for all simulations except those in Sect. 3.1 where the specified engine parameters will be changed to show the effect of higher compression ratios.

For consistency, we choose to compare all the losses with the engine operating at the same pressure. If the simulation produces a different average pressure from the starting pressure (7 MPa), the work output will be adjusted by the factor

$$W_{out} = \left(W_{out}\right)_s \cdot \frac{\overline{P}}{\overline{P}_w} , \tag{31}$$

where

$\overline{P}_w$ = average simulation pressure,

$\overline{P}$ = RE-1000 pressure (7 MPa),

$\left(W_{out}\right)_s$ = model simulation work output,

W_{out} = work output corrected to 7 MPa.

Equation (31) is approximately correct for ratios of $\overline{P}/\overline{P}_w$ close to one. Mean pressure is not the only basis of comparison that could have been chosen. Some researchers, for example, have specified that the mass of working fluid be constant when other conditions are changed. For our purposes, mean pressure is a convenient parameter to hold constant, and it may also be physically significant because it is the appropriate design parameter for an engine limited by creep strength.

Results of the simulation will be displayed in graphical form where possible to provide for easy interpretation. The numbers are tabulated in Appendix D for verification.

3.1 Adiabatic Loss

In this section, the effect of the adiabatic loss on engine performance will be shown for various engine compression ratios. The adiabatic loss, is a thermodynamic loss due to the temperature fluctuations in the working spaces. This loss is maximal when the cylinder spaces behave adiabatically because heat transfer in the cylinder moderates the temperature swing. This will be discussed further in Sect. 3.2. The loss will be shown by modeling the engine adiabatically, with no other losses, over a range of engine compression ratios.

The following changes were made to modify the RE-1000 parameters to produce these higher compression ratios. First, the dead volume was reduced. The volumes chosen are

Modified RE-1000

$$V_{dhm} = 1/2\ V_{dh} = 1.98 \times 10^{-5}\ m^3\ ,$$

$$V_{drm} = 1/2\ V_{dr} = 2.97 \times 10^{-5}\ m^3\ ,$$

$$V_{dcm} = 1/2\ V_{dc} = 1.47 \times 10^{-5}\ m^3\ ,$$

$$\overline{V}_c = 3/4\ \overline{V}_e = 4.77 \times 10^{-5}\ m^3\ .$$

These volume reductions decrease the dead volume and thereby increase the engine compression ratio.

To simulate a range of engine compression ratios, the prescribed piston and displacer amplitudes were varied; the higher the amplitude, the higher the compression ratio (due to larger volume swings). This was done by simulating the modified RE-1000 with different values of Y14 (motion amplitude ratio). This value was ranged from 0.2 to 1.0 (the measured value of Y14 for the RE-1000 is 0.667). This range of Y14 resulted in a compression ratio ranging from 1.13 to 1.89.

The above simulation was done for both adiabatic and isothermal cylinders (isothermal cylinders represent the no-loss case) with no other losses. The values used in this simulation are: Y14 = 0.2, 0.4, 0.6, 0.8, 1.0, adiabatic and isothermal cylinders, no other losses, Modified RE-1000 data. The results of these ten cases are shown in Figs. 3(*a*) and (*b*) and 4.

Figure 3(*a*) shows engine power output vs compression ratio for this modified RE-1000 engine. Two main points are indicated here: (1) the adiabatic cylinder engine produces more power than the isothermal cylinder one; and (2) this increase in power gets smaller at higher compression ratios. Thus, there seems to be a "best" case where the power output can be increased the most by having an adiabatic instead of an isothermal cylinder.

Figure 3(*b*) shows the engine efficiency vs compression ratio for both cylinders. This graph shows the effect of the adiabatic loss as the compression ratio is increased; not surprisingly, the graph indicates that the loss of efficiency due to adiabatic gas behavior in the cylinders increases as the compression ratio increases. Note that this loss certainly is not insignificant. For example, at CR = 1.89, the loss in efficiency is more than ten percentage points. This graph illustrates that a major drawback of high compression ratios is that they have much greater adiabatic efficiency loss than low compression ratio engines.

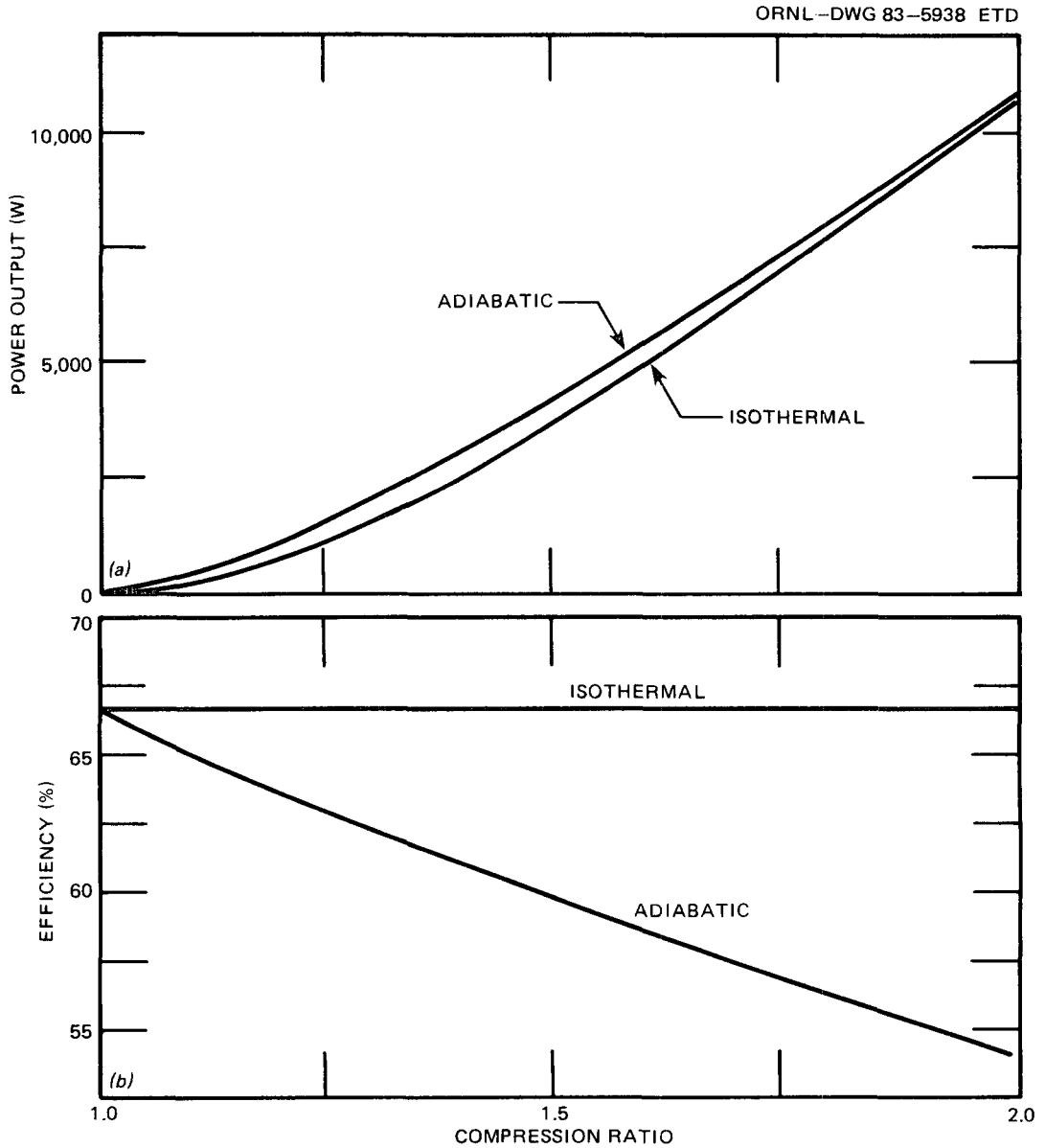

Fig. 3. (*a*) Power output vs compression ratio, and (*b*) efficiency vs compression ratio.

Figure 4 shows why this loss is higher. The temperature in the expansion space vs the phase angle of the power piston (i.e., the power piston position) is shown for various compression ratios. Note that, as the compression ratio increases, the temperature swing increases and the average temperature difference between the gas in the cylinder and the heater increases. The temperature in the compression space (not plotted) shows the same effect. That is, higher compression ratios will produce

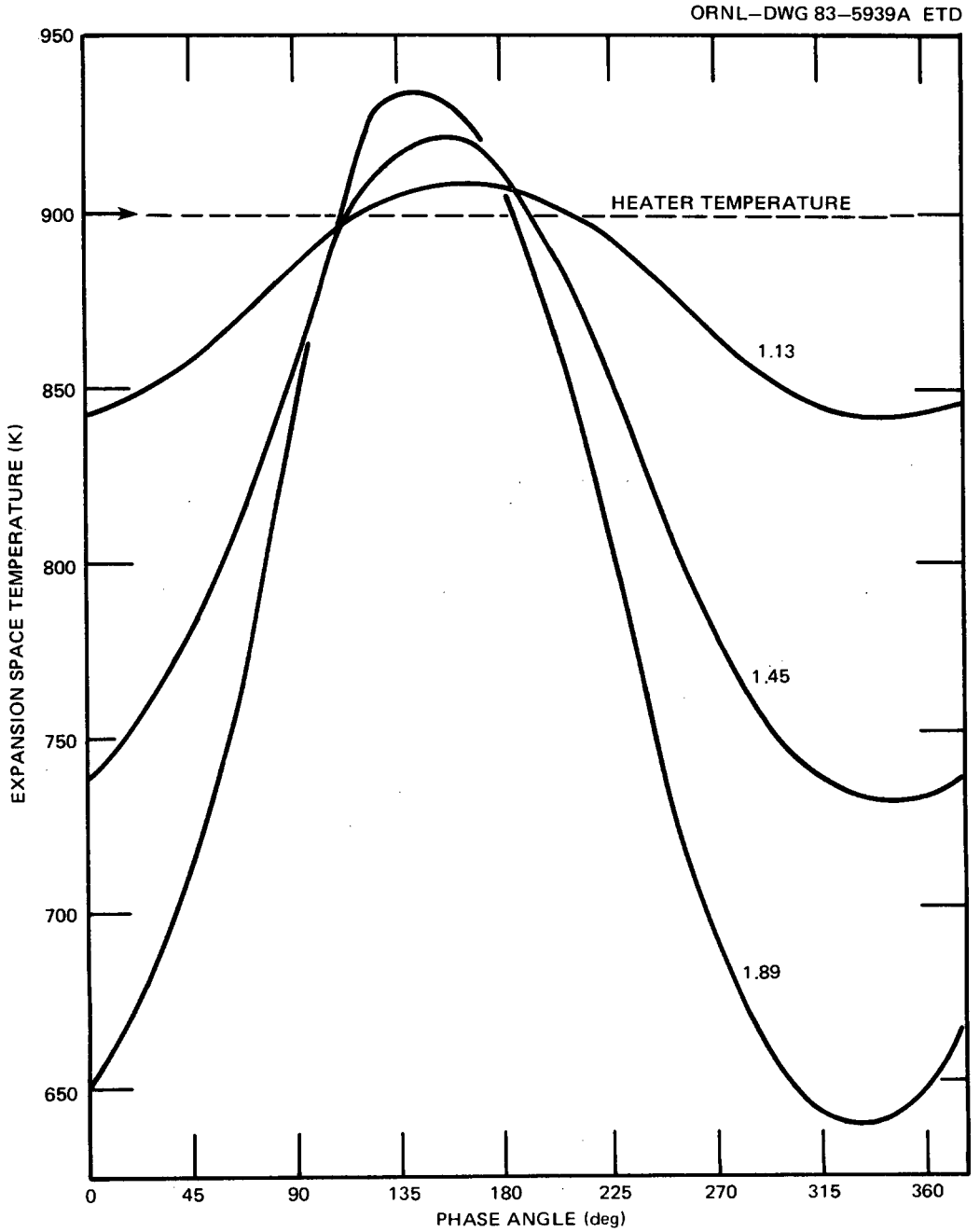

Fig. 4. Expansion space temperature vs phase angle.

higher temperature swings. These higher temperature swings, in turn, produce more adiabatic losses.

In conclusion, the following observations can be made about adiabatic loss in the RE-1000 engine: (1) the efficiency loss increases with increasing compression ratios, and (2) the power gain relative to isothermal cylinders at first increases, then decreases with increasing compression ratio.

3.2 Transient Heat Transfer Loss

This section will analyze the effect of the transient heat transfer loss on the engine performance. Adiabatic and transient heat transfer loss both exist simultaneously in the engine model except in the extreme cases ($h = 0$ and $h = \infty$). As noted before, the transient heat transfer loss occurs when there is heat transfer between the engine wall and the working fluid. The phenomenon not only causes a thermodynamic loss, but simultaneously reduces the adiabatic loss by moderating the temperature fluctuations. These thermodynamic losses will be shown by modeling the engine for a variety of transient heat transfer conditions with no other losses (except for adiabatic effects).

To simulate different transient heat transfer, the heat transfer coefficient will be varied; however, for simplicity, it will be assumed constant throughout the cycle and will be given the same value for both working spaces. By varying this coefficient from 0 (no heat transfer) to ∞ (instantaneous heat transfer) different degrees of the transient heat transfer loss can be demonstrated.

The above simulation was done for the RE-1000 engine with no other losses. The numbers used in the simulation are: h_e, h_c = 0, 10,000, 25,000, 62,500, 125,000, ∞ ($W/m^2 \cdot K$), program B, no other losses. The results are shown in Figs. 5(*a*) and (*b*) and 6.

Figures 5(*a*) and (*b*) show how engine performance changes with increasing heat transfer coefficient h. Figure 5(*a*) shows power output vs h, while 5(*b*) shows efficiency vs h. These two graphs show basically the same result; they both have a worst case. In other words, the power

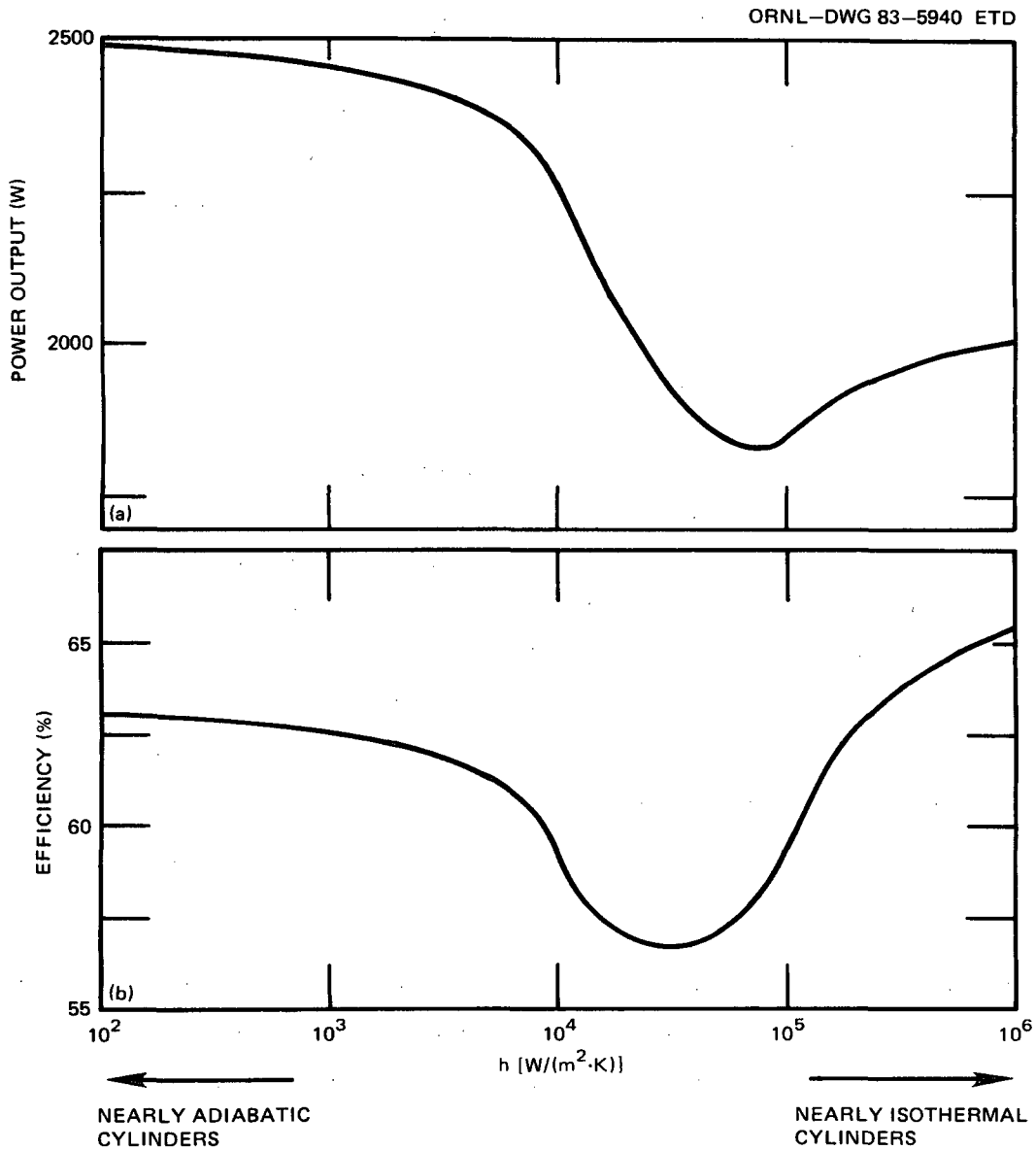

Fig. 5. (*a*) Power output vs h, and (*b*) efficiency vs h.

output and efficiency at first decrease, then increase as the heat transfer coefficient is increased from zero. Such a worst case was predicted earlier and is due to the effect of heat transfer moderating the temperature difference between the cylinder wall and the working gas.

This moderation of temperature difference by heat transfer is shown by Fig. 6. Expansion space temperature vs phase angle (i.e., piston position) is shown for various values of h. The tendency is clear that increasing h reduces the temperature swing in this space. Thus, increasing

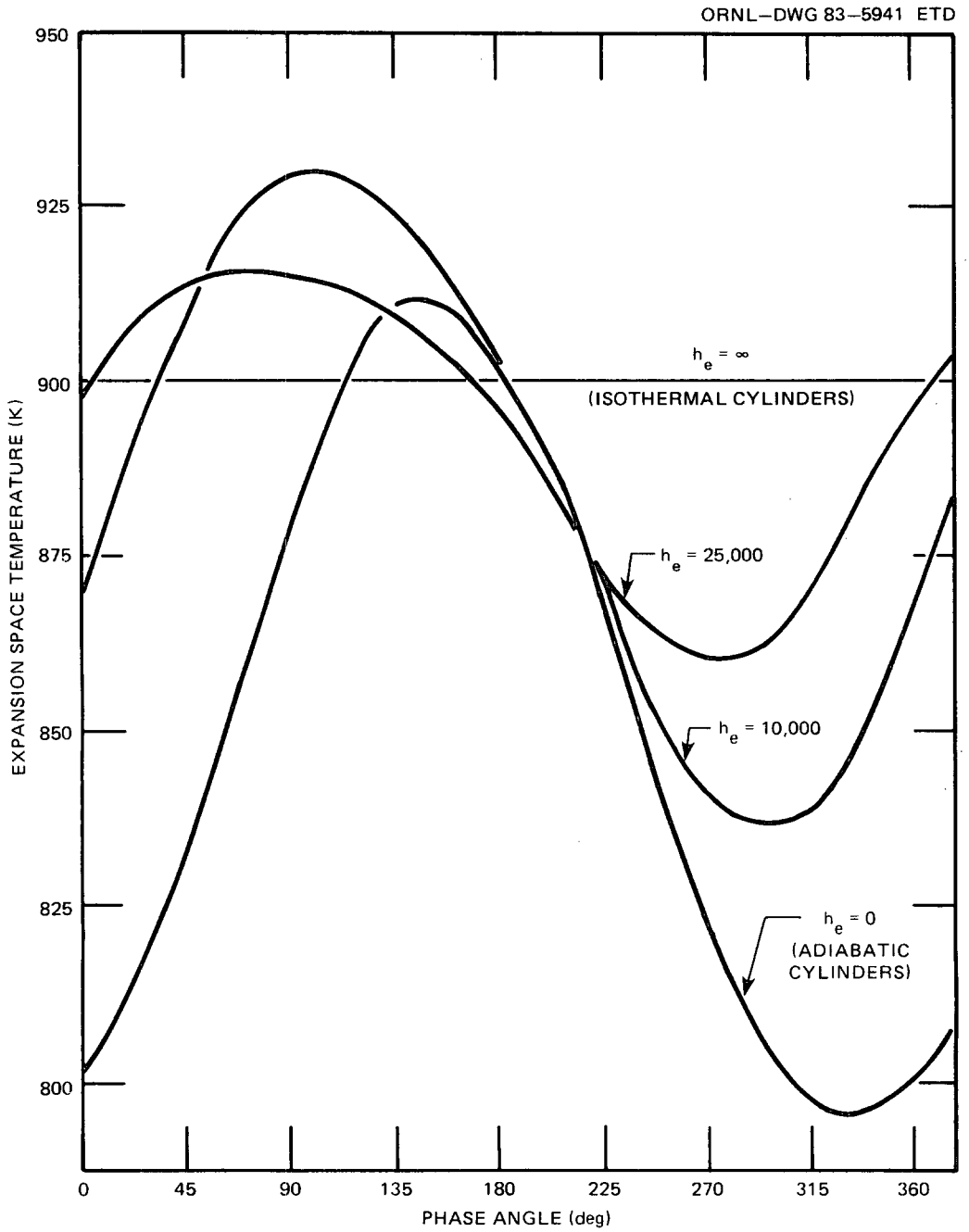

Fig. 6. Expansion space temperature vs phase angle.

h will at first increase the transient heat transfer loss due to a higher coefficient. This loss, however, will then hit a maximum and decrease to zero because the temperature difference approaches zero at very high values of h.

One other observation comes from Fig. 6. Since the temperature swings decrease as h increases, the adiabatic loss will also decrease as h increases. Therefore, the engine should be more efficient when operating isothermally than when operating adiabatically [Fig. 5(*b*)].

In conclusion, the following statements are supported by these results.

1. There is a worst case for both power output and efficiency for a certain value of h.
2. Increasing h tends to moderate the temperature swings and reduce the difference between the average gas temperatures and the adjacent heat exchanger temperatures.
3. Increasing transient heat transfer reduces the adiabatic loss.

3.3 Pressure Drop Loss

The analysis of pressure drop losses will be explored in this section. This loss is basically a flow loss caused by the working gas losing pressure while it is flowing through the dead volume (heat exchanger components). The analysis will involve evaluating these losses for various degrees of pressure drop.

The pressure drop is represented by Eqs. (17) and (18).

$$\frac{dm_e}{dt} = k_{de} \left(P_d - P_e\right)^{n_{de}} , \tag{17}$$

$$\frac{dm_c}{dt} = k_{dc} \left(P_d - P_c\right)^{n_{dc}} + k_{bc} \left(P_b - P_c\right)^{n_{bc}} . \tag{18}$$

The equations show that the loss is controlled by two different types of constants (recall that for pressure drop only, $k_{bc} = 0$), one of which is the flow coefficient (k_{de}, k_{dc}). This value basically controls the amount of pressure drop loss in a given simulation. Different degrees of pressure drop are shown by varying this coefficient from ∞ (no pressure drop) to 0 (maximum pressure drop or no flow).

The other loss-controlling coefficient is the pressure drop exponent (n_{de}, n_{dc}). This exponent essentially represents the nature of the flow.

When n_{de} and $n_{dc} = 1$, the flow is said to be laminar and the correlation is linear. When $0.5 < n_{de}, n_{dc} < 1.0$, the flow is said to be in transition or turbulent, and the correlation is nonlinear. Using the linear correlation is usually analytically simpler and fairly accurate for the regenerator, which is usually the major source of pressure drop. Experimental data, however, indicate that a nonlinear correlation is a more accurate representation of the flow in general, and particularly in the heater and cooler. How these correlations compare is important to any effective analysis of this engine.

To show pressure drop, the engine will be simulated by varying the value of k, the flow coefficients over the range of ∞ to 0, or until the computed power output becomes negative. For simplicity, k's in both equations will be assumed to be the same. This will be done for both a linear and nonlinear pressure drop correlation. For the nonlinear pressure drop correlation, the following value of n will be used:

$$n_{de} = n_{dc} = 1/1.75 \ .$$

Such a value, although not necessarily totally accurate, is believed better than a linear approximation for this combination of turbulent/oscillating flow.

The calculation was performed for both adiabatic and isothermal cylinders. Isothermal cylinders were used because this simulation would simulate the engine with only pressure drop losses. However, adiabatic cylinders were assumed in a typical machine because the cylinders are more nearly adiabatic than isothermal.[3]

The following input values were used:

<u>Pressure drop calculation (linear)</u>

$$k_{de}, k_{dc} = 0.75 \times 10^{-7},\ 1 \times 10^{-7},\ 1.5 \times 10^{-7},\ 2 \times 10^{-7},\ 3 \times 10^{-7}\ \mathrm{kg/(s \cdot Pa)}\ ,$$

$$n_{de}, n_{dc} = 1.0 \ .$$

Isothermal and adiabatic cylinders, program A.

Pressure drop calculation (nonlinear)

$$1/k_{de},\ 1/k_{dc} = 13{,}333,\ 20{,}000,\ 30{,}000,\ 40{,}000,\ 50{,}000\ [kg/(s \cdot Pa^{0.57})]^{-1}$$

$$n_{de},\ n_{dc} = 1/1.75\ .$$

Isothermal and adiabatic cylinders, program A.

The results are shown on Figs. 7(*a*) and (*b*), 8(*a*) and (*b*), and 9(*a*) and (*b*).

Figures 7(*a*) and (*b*) show how linear pressure drops affect calculated engine performance. Figure 7(*a*) shows power output vs 1/k, while Fig. 7(*b*) shows efficiency vs 1/k for both cylinders.

Two observations can be drawn from these graphs: (1) Although the graphs are not exactly linear (the efficiency curves especially show some curvature), they are linear enough to be represented adequately by straight lines. (Such linear curves would seem to suggest that nonlinear effects in the equations are not very significant for this particular case); and (2) In Fig. 7(*b*), the isothermal and adiabatic curves cross. Such an effect does not occur in Fig. 7(*a*), which suggests that for high pressure drops, both the engine power output and the efficiency can be increased by having an adiabatic cylinder. Adding the adiabatic loss improves engine performance if the pressure drop is sufficiently high to make the performance very poor anyway.

Exactly why the curves cross is shown in Figs. 8(*a*) and (*b*). In Fig. 8(*b*), the pressure in the expansion space vs crank angle is plotted for an adiabatic cylinder, while the same axes are plotted for the isothermal cylinder in Fig. 8(*a*). The two curves plotted in each graph are for no pressure drop ($k = \infty$) and a large pressure drop (in this case $k = 1.0 \times 10^{-7}$ kg/Pa•s). Basically the graphs show that the pressure curve is less affected by pressure drop for an adiabatic cylinder than for an isothermal cylinder. The power output and the efficiency (which is proportional to the pressure since dV does not change) for an adiabatic cylinder does not drop off as fast as for an isothermal cylinder. The pressure drop loss does not affect an adiabatic cylinder as much as an isothermal one.

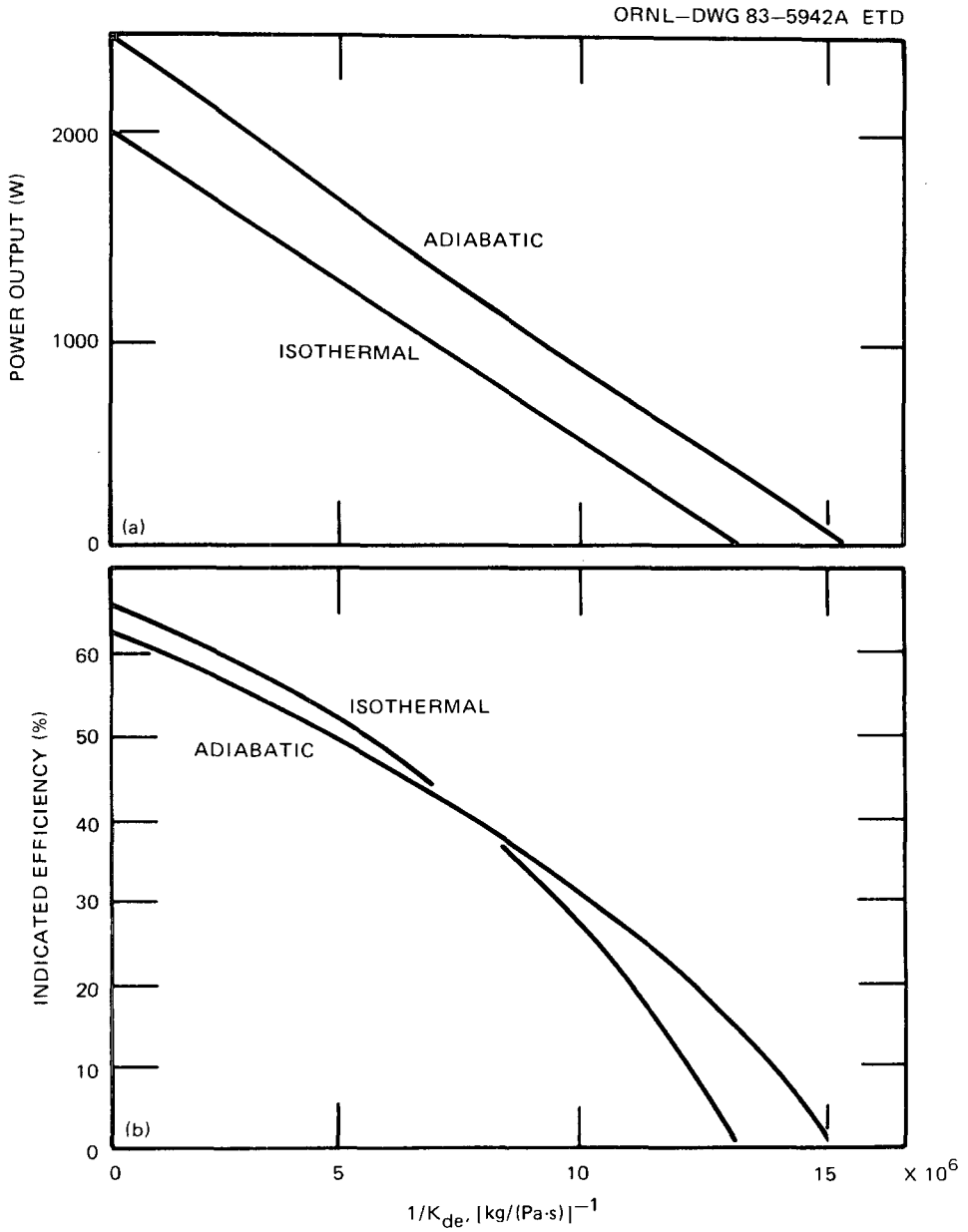

Fig. 7. (*a*) Power output vs $1/k_{de}$, $1/k_{dc}$ (linear correlation), and (*b*) efficiency vs $1/k_{de}$, $1/k_{dc}$ (linear correlation).

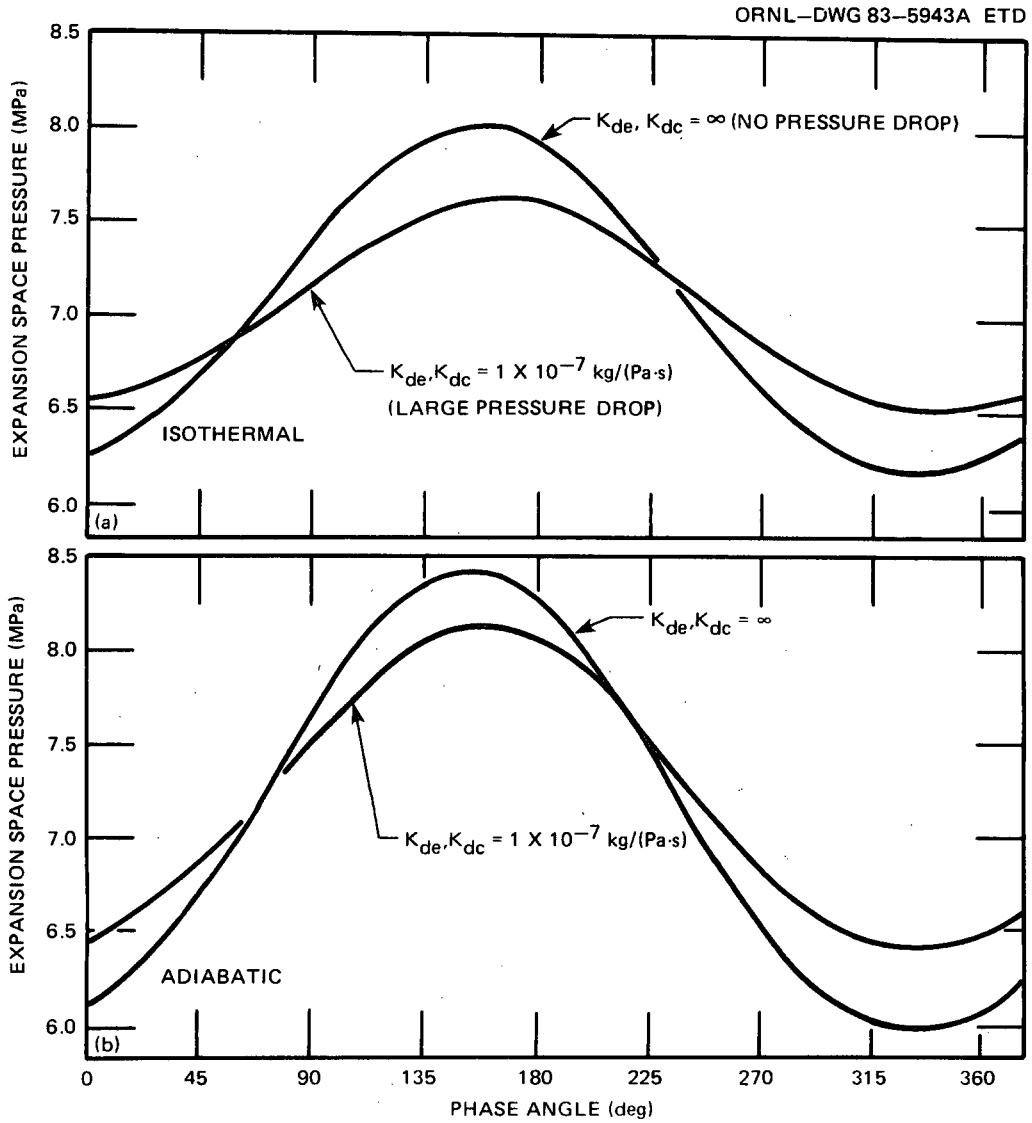

Fig. 8. (*a*) Expansion space pressure vs phase angle (isothermal), and (*b*) expansion space pressure vs phase angle (adiabatic).

The effect of nonlinear correlations on engine performance is shown in Figs. 9(*a*) and (*b*). Figure 9(*a*) shows power output vs 1/k, while Fig. 9(*b*) shows efficiency vs 1/k. The graphs are similar to those in Figs. 7(*a*) and (*b*) that have a linear correlation. The curve shapes, however, now possess noticeable curvature. This would seem to indicate that the nonlinearity of the correlation has an important effect on predicted engine performance and one might conclude that linear approximations to

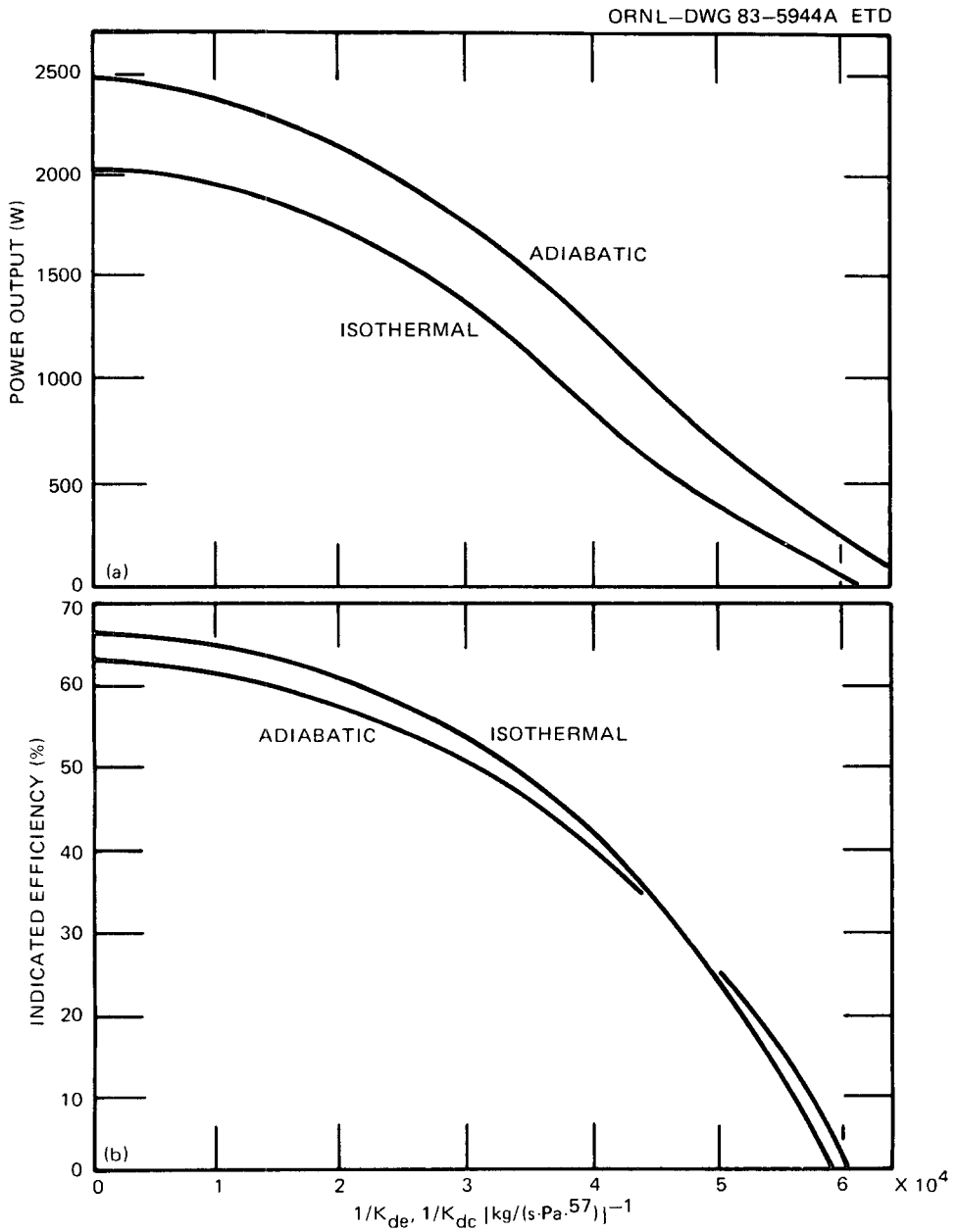

Fig. 9. (*a*) Power output vs $1/k_{de}$, $1/k_{dc}$ (nonlinear correlation), and (*b*) efficiency vs $1/k_{de}$, $1/k_{dc}$ (nonlinear correlation).

this nonlinear correlation probably will not yield totally accurate results.

In conclusion the following results are supported by this analysis.

1. The loss in engine performance is almost proportional to 1/k, at least if the pressure drop is a linear function of mass flow rate.
2. The pressure drop loss has a larger effect on an isothermal cylinder than on an adiabatic cylinder.
3. Nonlinear pressure drop correlations affect engine performance differently from linear correlations.

3.4 Seal Leakage Loss

Seal leakage loss, like pressure drop, is also a kind of flow loss. However, it affects engine performance somewhat differently. This loss will be shown by solving the equations numerically for various degrees of seal leakage.

The seal leakage loss is shown in this model by Eq. (19), which is repeated below.

$$\frac{dm_w}{dt} = k_{bc} \left(P_b - P_c\right)^{n_{bc}} . \tag{19}$$

Because Eq. (19) is similar in form to the pressure drop loss discussed in the previous section, it can be modeled in a similar fashion.

As with pressure drop, the amount of loss will be shown by varying k_{bc}. For this loss, the range is from 0 (no flow loss) to ∞ (no seal) or until the engine power output becomes negative. A linear correlation ($n = 1$) and a nonlinear correlation ($n \neq 1$) will also be simulated to show the effects of nonlinear pressure drop correlations. The following value for n will be used for a nonlinear correlation $n_{bc} = 1/1.75$. This value was chosen because it would better represent the turbulent/oscillating flow that actually occurs in a real engine than would a linear correlation.[2]

The simulation was done for both isothermal and adiabatic cylinders. As in the pressure drop analysis, isothermal cylinders were used to show the effects of seal leakage loss acting alone, while adiabatic cylinders

were used because most real Stirling engines actually operate more nearly adiabatically than isothermally.[3] This calculation was done for the following input values.

Seal leakage calculation (linear)

$k_{bc} = 0.5,\ 1,\ 2,\ 3 \times 10^{-8}$ kg/Pa•s

$n_{bc} = 1$

Isothermal and adiabatic cylinders, program B.

Seal leakage calculation (nonlinear)

$k_{bc} = 25,\ 50,\ 75,\ 100,\ 125 \times 10^{-7}$ (kg/s•$Pa^{0.75}$)

$n_{bc} = 1/1.75$

Isothermal and adiabatic cylinders, program B.

The results of the above simulations are shown in Figs. 10(*a*) and (*b*), 11(*a*) and (*b*), and 12(*a*) and (*b*). Each graph is explained below.

Figures 10(*a*) and (*b*) show the effect of seal leakage on engine performance. Figure 10(*a*) shows power output vs k_{bc}, while 10(*b*) shows efficiency vs k_{bc}. In many ways, these graphs are similar to the pressure drop results because they are surprisingly linear, especially at the smaller values of k_{bc}. This would suggest that the nonlinear terms in the equations have little effect on the solution.

These graphs show an interesting characteristic; that is, the isothermal and adiabatic curves cross on Fig. 10(*a*), but not on Fig. 10(*b*). This result indicates that at high mass leakage rates, more power output and efficiency can be achieved by having an isothermal cylinder; that is, more power can be generated by an isothermal cylinder than an adiabatic one, with no sacrifice in efficiency — but only if the power is low anyway due to excessive piston leakage. This was not seen in the pressure drop analysis. Such a result indicates that even though the two losses are represented by a mathematically similar expression, they affect engine performance differently.

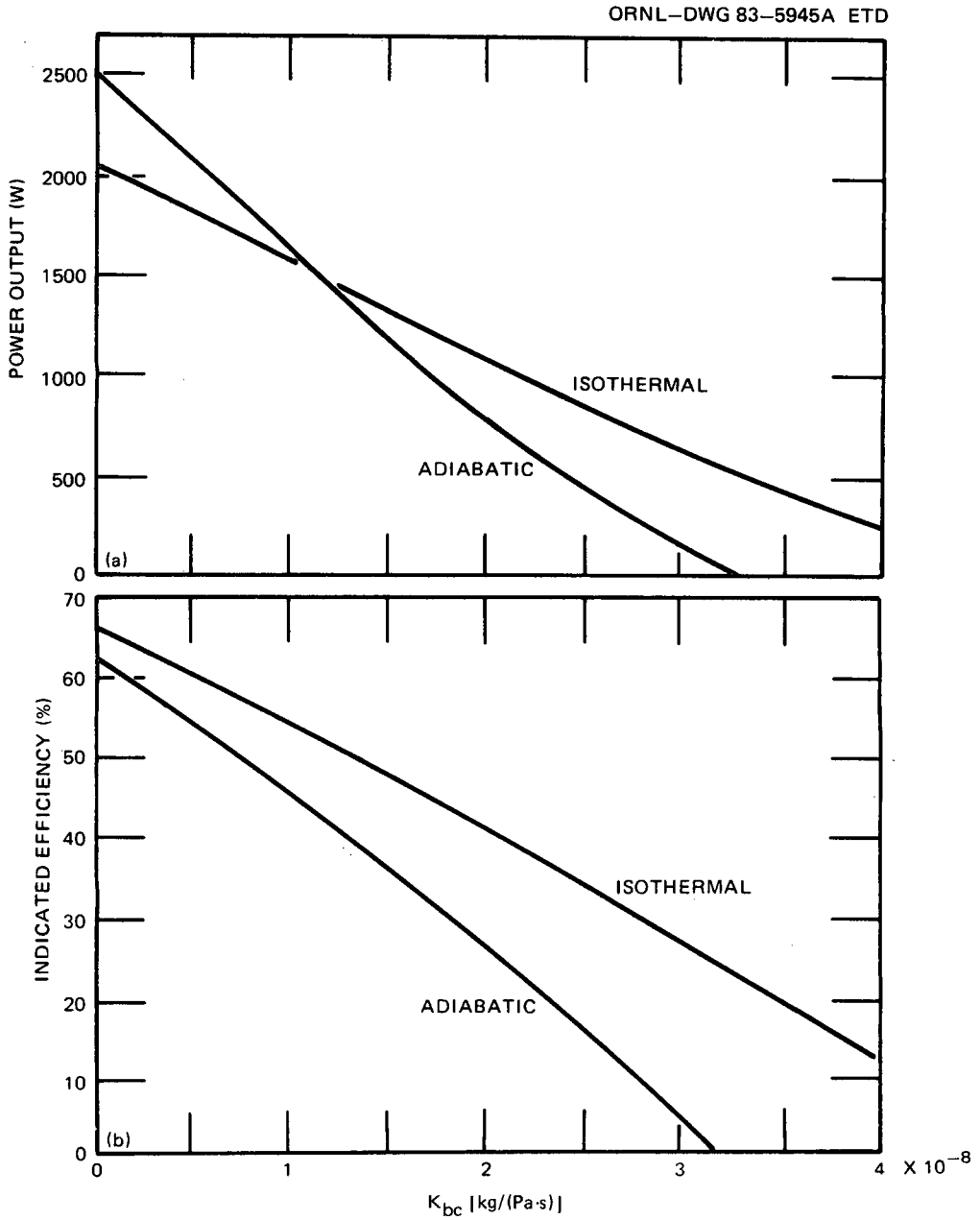

Fig. 10. (*a*) Power output vs k_{bc} (linear correlation), and (*b*) efficiency vs k_{bc} (linear correlation).

Exactly why the curves cross is shown in Figs. 11(*a*) and (*b*). In Fig. 11(*a*), the pressure wave in the expansion space is plotted vs crank angle for an isothermal cylinder while the same plot for an adiabatic cylinder is shown in Fig. 11(*b*). The two curves plotted in each graph are for no seal leakage (k_{bc} = 0) and high seal leakage ($k_{bc} = 3 \times 10^{-8}$).

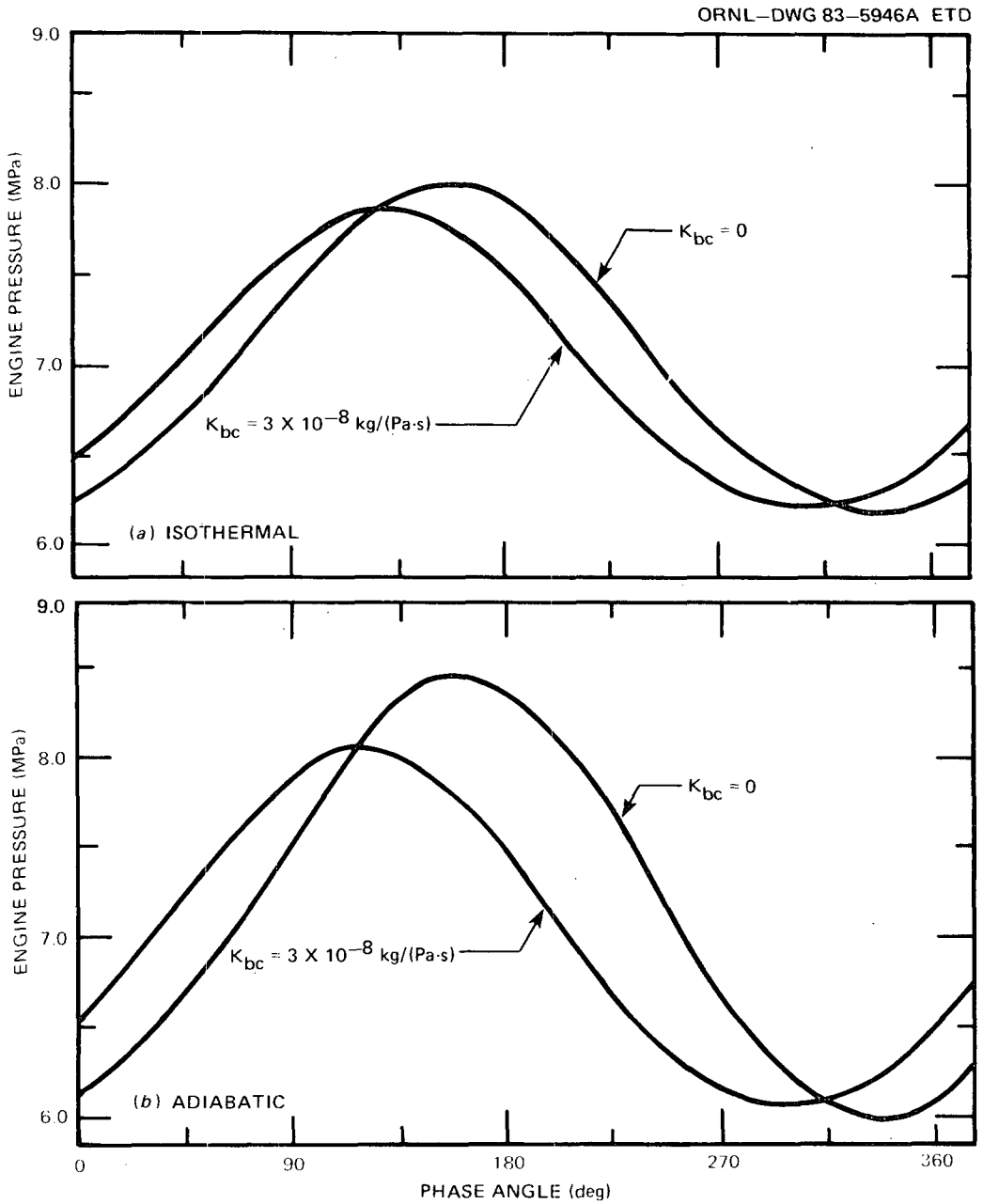

Fig. 11. (*a*) Pressure vs phase angle (isothermal), and (*b*) pressure vs phase angle (adiabatic).

The graphs show that seal leakage has a greater effect on the pressure wave in an adiabatic cylinder than in an isothermal cylinder. This is not surprising because seal leakage depends on the pressure difference between the engine and the bounce space, and the engine pressure variation is larger with adiabatic cylinders. Because power output is a

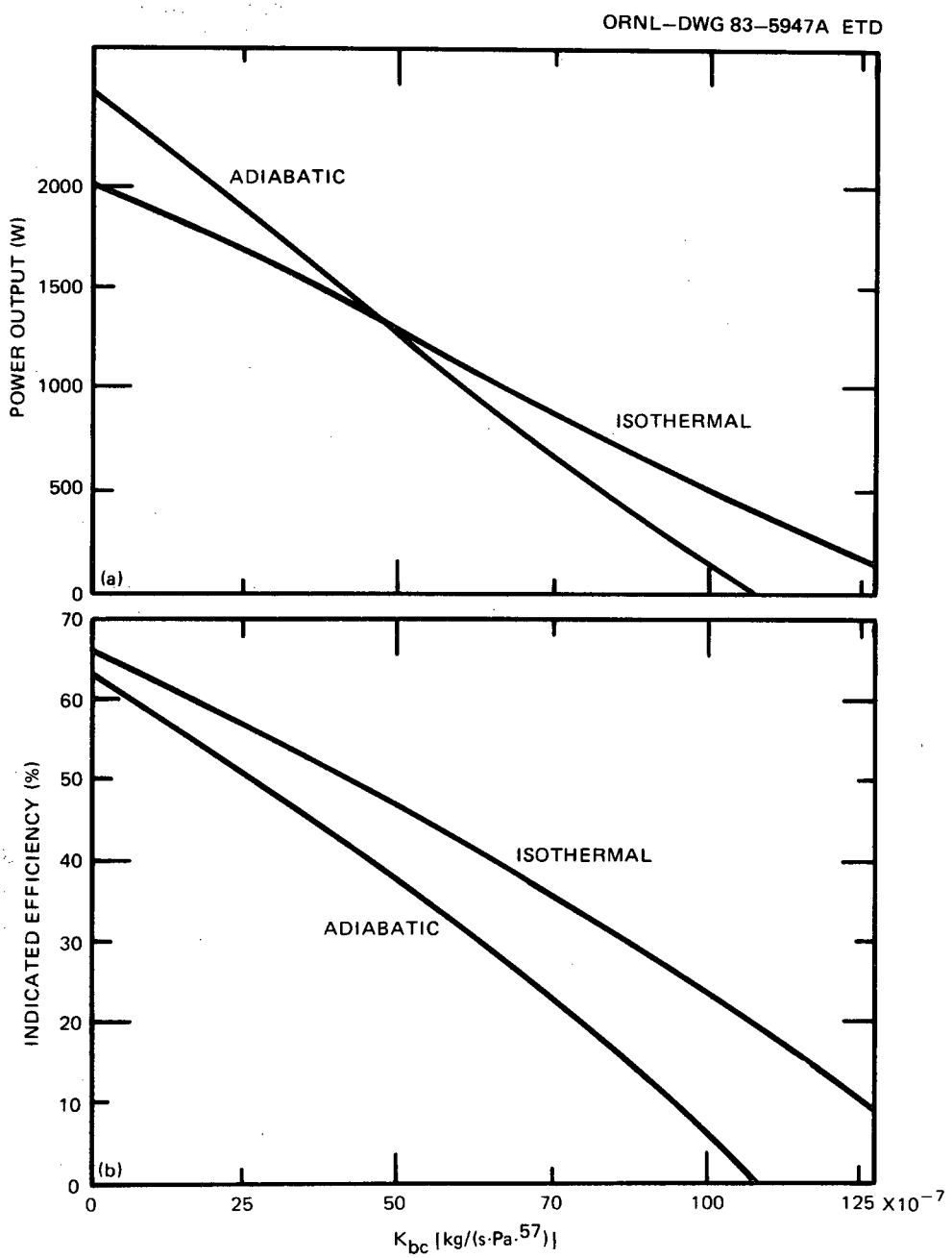

Fig. 12. (*a*) Power output vs k_{bc} (nonlinear correlation), and (*b*) efficiency vs k_{bc} (nonlinear correlation).

function of the pressure wave only (for a given swept volume of the pistons), the seal leakage loss affects the adiabatic cylinders power output more than that of an isothermal cylinder. As a result, the efficiency curves diverge while the power output curves converge and, eventually, cross.

The effect of using nonlinear correlations on engine performance is shown in Figs. 12(*a*) and (*b*). Figure 12(*a*) shows power output vs k_{bc}, while 12(*b*) shows efficiency vs k_{bc}. Basically, the graphs are similar to the linear correlation graphs. In fact, the curve shapes hardly change. This was not the case in the pressure drop analysis where the plots showed changes in curvature. This result would thus suggest that nonlinear mass leakage correlations can be reasonably accurately represented by linear correlations.

The following statements are supported by these results.

1. The seal leakage loss effect on engine performance is almost proportional to the leakage coefficient.
2. Seal leakage loss has a larger effect on adiabatic cylinders than on isothermal cylinders.
3. Nonlinear correlations affect engine performance in much the same manner as linear correlations.

3.5 Coupled Loss Analysis

This section will determine the degree of coupling of the pressure drop and seal leakage losses. As stated before, these losses are certainly coupled in reality. The exact extent of coupling will indicate, in one respect, the necessity of third-order codes (which can simulate this coupling). The degree of coupling of these two losses will be estimated by simulating the model in a coupled mode.

To estimate the effect of coupling, the effect of the losses must be quantified. This will be done by taking the difference between the power output with the loss and the power output without the loss. In other words,

$$P_L = P_{nl} - P_{wl} , \tag{32}$$

where

P_L = power loss due to the loss mechanism;
P_{nl} = power output, no loss case;
P_{wl} = power output with the loss.

A coupling factor (CF) can then be defined.

$$CF = \frac{(P_{LS} + P_{LP}) - P_{L(S + P)}}{P_{L(S + P)}}, \tag{33}$$

where

P_{LS} = power loss due to the seal leakage acting alone (decoupled),

P_{LP} = power loss due to pressure drop acting alone (decoupled),

$P_{L(S + P)}$ = power loss due to both modeled simultaneously (coupled).

This factor will basically show the degree to which the losses affect each other while they are present simultaneously. The greater the CF deviates from zero, the more the losses are coupled. Any CF close to zero would indicate that modeling the losses individually (i.e., with a decoupled or second-order calculation) could be fairly accurate.

The previous analysis was completed only for combinations of pressure drop and seal leakage losses because the adiabatic and transient heat transfer losses cannot be represented by Eq. (33). To perform this kind of analysis with these losses, an analysis involving reversible work would have to be completed on the working spaces.

The analysis was performed for one value of k_{de}, k_{dc}, and k_{bc}. Linear pressure drop correlations were used. The analysis was done for adiabatic cylinders (h = 0), isothermal cylinders (h = ∞), and semi-adiabatic cylinders (h = 62,500 $W/m^2 \cdot K$). The input quantities for each case are shown below.

Coupled loss analysis

Case 1	No losses	$k_{bc} = 0$	$k_{de}, k_{dc} = \infty$
	Mass leakage	$k_{bc} = 1 \times 10^{-8}$	$k_{de}, k_{dc} = \infty$
(h = 0)	Pressure drop	$k_{bc} = 0$	$k_{de}, k_{dc} = 1.5 \times 10^{-7}$
	Both losses	$k_{bc} = 1 \times 10^{-8}$	$k_{de}, k_{dc} = 1.5 \times 10^{-7}$
Case 2	Same input		
(h = ∞)			
Case 3	Same input		
(h = 62,500)			

All three cases basically show the same result. Table 1 shows the coupling result for all three cases. The main result here is that the coupling factors for all three cases are close to zero. The worst case is for h = 62,500; however, even here the coupling factor is only 0.032.

Table 1. Coupled loss analysis

K_{bc} (kg/Pa•s)	$1/k_{de}$, $1/k_{dc}$ (Pa•s/kg)	W_{out} (W)	P_{loss} (W)
Case 1 (adiabatic case, h = 0)			
0	0	2496	0
1×10^{-8}	0	1605	891
0	6.66×10^{6}	1393	1103
1×10^{-8}	6.66×10^{6}	562	1934

$$CF = \frac{891 + 1103 - 1934}{1934} = 0.0310$$

Case 2 (isothermal case, h = ∞)			
0	0	2031	0
1×10^{-8}	0	1562	469
0	6.66×10^{6}	1010	1021
1×10^{-8}	6.66×10^{6}	565	1466

$$CF = \frac{469 + 1021 - 1466}{1466} = 0.0164$$

Case 3 (finite heat transfer rate, h = 62,500 W/m²•K)			
0	0	1840	0
1×10^{-8}	0	1242	598
0	6.66×10^{6}	816	1024
1×10^{-8}	6.66×10^{6}	268	1572

$$CF = \frac{598 + 1024 - 1572}{1572} = 0.0318$$

For this engine, the coupling between these two losses is minimal. This means second-order codes can be quite accurate for evaluating these losses simultaneously for this particular case.

In conclusion, the coupling of the pressure drop and seal leakage loss is probably minimal, and therefore second-order codes are applicable to this engine.

4. SUMMARY

This section provides some discussion and recommendations based on the results of this study. In this section, the following points will be discussed: (1) the validity of the results produced by the model, (2) the positive and negative points of this computer solution to this model, and (3) topics for further study.

The validity of the results cannot be determined on the basis of these results alone; for true validation, experimental evidence should be used for comparison. Yet, some estimate can be made based on the model's assumptions. For instance, one critical assumption was that piston variation can be described by prescribed sinusoidal motion. Such an assumption completely eliminates dynamic effects on the engine solution. These dynamic effects could be critical to the problem solution, and thus remain to be explored. In any case, there will be some sacrifice in accuracy because of this assumption.

Another critical assumption was that the working gas was well mixed in the expansion and compression spaces. Again, this is most certainly not exactly true for a real engine. In actuality, this model tries to take into account these effects by lumping them into loss coefficients. For instance, the heat transfer coefficient represents the sharp temperature gradient that exists at the engine cylinder wall. Obviously, though, this phenomenon is described by more complicated relations. Thus, these two assumptions are certainly approximations in the formulation and therefore in the results.

The use of the CSMP subroutine to solve the equations had both positive and negative aspects. On the positive side, it provided an adequate solution to this model with nonlinear effects accounted for. Thus, accuracy to within the limits of validity of the theoretical formulation could be assumed. Such accuracy was also achieved with minimal programming effort because the CSMP subroutine provided block statements that eliminated many programming tasks. This solution was also relatively quick and fairly inexpensive (the computer program required an average of 10 CPU seconds for each case). Thus, this program is advantageous in the sense

that accurate solutions to the model were provided quickly and cheaply with minimal programming effort.

The main disadvantage in using the prepackaged programs was that the solution was constantly plagued by numerical problems. The two main problems were numerical instability and round-off error. The instability problem occurred when low pressure drop or high heat transfer coefficients were specified. These cases cannot thus be simulated. The round-off error occurred whenever integrations for average expansion space temperatures were evaluated. As a result, average expansion space temperatures could not always be evaluated very accurately. Thus, the program is good at obtaining accurate solutions only within these restrictions.

These results do suggest some topics for further study. One is the continued verification of this engine model. As noted before, no real conclusions can be drawn on the validity of the results until quantitative comparisons with experimental data are made (although the trends and major effects predicted are all consistent with experimental experience). Therefore, a verification study should be done for this formulation by comparing the model simulation with experimental results.

Another topic for further analysis is to expand the model so that engine dynamics are included. The necessary additional formulation required is relatively minor for this extension. It would involve the addition of two dynamic equations for two unknowns (piston and displacer positions). The additional programming effort would also be rather small. However, achieving adequate simulations could be a problem because the loss mechanisms suddenly play an important role in the engine steady state operation. This is especially true for the pressure drop loss. As a result, the loss coefficients cannot be assigned values as arbitrarily as in this study. Such an analysis should be more accurate, because dynamic effects are now considered in the formulation. Furthermore, the numerical problems (which are completely absent from the ORNL linear harmonic analysis[5]) are likely to be even more troublesome when the dynamic effects are included.

In conclusion, this analysis was successful both in providing a numerical solution that can solve the engine model formulation without simplification and in demonstrating how this model will predict the effect

of the four previously stated loss mechanisms on engine performance. The analysis also showed that the CSMP subroutine can be used effectively in model simulation of this kind. The nonlinear analysis was completely successful in its objective of providing results for comparison with the newly developed ORNL linear harmonic analysis. However, further analysis may be needed. Model verification by experimental data and the addition of dynamic effects are the next steps in the total analysis of this engine formulation. Such future work would help to show whether this formulation is an accurate predictor of engine operation.

REFERENCES

1. J. Van Wylen and R. E. Sonntag, *Fundamentals of Classical Thermodynamics*, 2d ed., John Wiley and Sons, Inc., New York, 1973.

2. J. Schreiber, *Testing and Performance Characteristics of a 1-kW Free-Piston Stirling Engine*, NASA Technical Memorandum 82999, 1983.

3. G. Walker, *Stirling Engines*, 1st ed., Clarendon Press, Oxford, 1980.

4. F. H. Speckpart and W. L. Green, *A Guide to Using CSMP — The Continuous System Modeling Program*, Prentice Hall, Inc., Englewood Cliffs, N.J., 1976.

5. N. C. J. Chen, F. P. Griffin, and C. D. West, *Linear Harmonic Analysis of Stirling Engine Thermodynamics*, ORNL/CON-155, to be published at Oak Ridge National Laboratory.

Appendix A

PROGRAM LISTING

Both program A (pressure drop program) and program B (no pressure drop program) are listed in FORTRAN language. These programs must be used in conjunction with the CSMP III subroutine. Calling up this subroutine is done with control cards. This procedure varies depending on the computer. For the computer located at Oak Ridge National Laboratory, the following sequence can be used:

```
(Job card)
(Password)
EXEC CSMPIII
SYSUDUMP DO DUMMY
X SYSIN DO*
```

Additional information on the CSMP III is available in Ref. 1.

A.1 Program A Listing

Program A (minus control cards)

```
Title       RE-1000 Analysis — An Ideal Kinematic Mode
C           The initial section inputs the initial conditions and engine
            constants.

Initial

1           Dimension AQIN (500), AQOUT (500), ...
            AATE (500), AATC (500), AAPE (500), ...
            AAPC (500), AAPD (500)
            FIXED N, M
C           The following cards are input conditions.
            INCON THEAT =
            INCON TCOOL =
            CONSTANT KDE =       , KDC =
            CONSTANT NDE =       , NDC =
            CONSTANT KBC =
            CONSTANT NBC =
            CONSTANT HE =        , HC =
C           The following cards are engine parameters.
            XPMAX = 0.0202
            XDMAX = 0.0210
            AD = 0.002572
```

```
      AP = 0.002572
      AR = 0.00218
      VEAVG = 0.0000636
      VCAVG = 0.0001036
      VDH = 0.0000396
      VDR = 0.0000594
      VDC = 0.0000285
      DP = 0.05723
      DD = 0.05723
      FH = 30
      BDD = 45
      PWAVG = 7,000,000
      PB = 7,000,000
      ASEAVG = 0.01392
      ASCAVG = 0.02292
      Y14 = 0.667
      XDXP = 1
      CP = 5200.
      R = 2080.
      PI = 3.1416
C     The following cards calculate other engine parameters for all
      time.
      CV = CP-R
      G = CP/CV
      GM1 = G-1
      XPAMP = XPMAX*Y14
      XDAMP = XPAMP*XDXP
      TREG = (THEAT-TCOOL)/ALOG (THEAT/TCOOL)
      VDAVG = VDH + VDR + VDC
      TDAVG = VDAVG/(VDH/THEAT + VDR/TREG + VDC/TCOOL)
      FR = FH*2*PI
      B = BDD*PI/180.
C     The following cards calculate other engine parameters at time
      t = 0.
      VES = VEAVG — AD*SIN(B)
      VCS = VCAVG + (AD — AR)*SIN(B)
      MES = VEAVG*PWAVG/R/THEAT
      MCS = VCAVG*PWAVG/R/TCOOL
      MDS = VDAVG*PWAVG/R/TDAVG
      MWS = MES + MCS + MDS
      TE = THEAT
      TC = TCOOL
      ME = MES
      MC = MCS
      MD = MDS
      MW = MWS
      VEOLD = VES
      VCOLD = VCS
      PEOLD = PWAVG
      PCOLD = PWAVG
      PDOLD = PWAVG
```

```
C           The following cards are program control cards.
            AVGTE = 0.
            AVGTC = 0.
            AVGPE = 0.
            AVGPC = 0.
            AVGPD = 0.
            POIN = 0.
            POUT = 0.
            WOUT = 0.
            EFF = 0.
            PSTEP =
            M =
            N = 1
            XTIME = 1
C           The dynamic segment simulates the model.  The nosort card is
            required due to the FORTRAN logic programming.
DYNAMIC
NOSORT
C           The following cards are the algebraic part of the formulation.
            TSTEP = TIME — XTIME
            XP = XPAMP*SIN (FR*TIME)
            XD = XDAMP*SIN (FR*TIME + B)
            VE = VEAVG — AD*XD
            VC = VCAVG + (AD — AR)*XD — AP*XP
            DVE = (VE — VEOLD)/TSTEP
            DVC = (VC — VCOLD)/TSTEP
            VTOT = VE + VC + VDAVG
            PE = ME*R*TE/VE
            PEN = (PEOLD + PE)/2
            PC = MC*R*TC/VC
            PCN = (PCOLD + PC)/2
            PD = MD*R*TDAVG/VDAVG
            PDN = (PD + PDOLD)/2
            PEDVE = PEN*DVE
            PCDVC = PCN*DVC
C           The following cards are the differential equations part of the
            program.
            PDEDE = (PD — PE)*KDE*(ABS (PD — PE)**NDE/ABS (PD — PE)
            PDEDC = (PD — PC)*KDC*ABS (PD — PC)**NDC/ABS (PD — PC)
            MLEBC = (PB —PC)*KBC*ABS (PB — DC)**NBC/ABS(PB — PC)
            DME = PDEDE
            ME = INTGRL (MES, DME)
            DMC = PDEDC + MLEBC
            MC = INTGRL (MCS, DMC)
            DMD = —PDEDE -PDEDC
            MD = INTGRL (MDS, DMD)
            MW = ME + MC + MD
            FE = INSW (DME, 1.0, 0)
            FC = INSW (DMC, 1.0, 0)
            TFE = FE*TE + (1. — FE)*THEAT
            TFC = FC*TC + (1. — FC)*TCOOL
            ASE = ASEAVG
```

```
      ASC = ASCAVG
      V1 = -TE*DME/ME - GM1*TE*DVE/VE + G*DME*TFE/ME +
      HE*ASE*(THEAT - TE)/CV/ME
      TE = INTGRL (THEAT, V1)
      V2 = -TC*DMC/MC - GM1*TC*DVC/VC + G*DMC*TFC/MC +
      HC*ASC*(TCOOL - TC)/CV/MC
      TC = INTGRL (TCOOL, V2)
C     The following cards integrate TE, TC, PE, PC, PD, PEDVE, and
      PCDVC.
      ATE = INTGRL (0.0, TE)
      ATC = INTGRL (0.0, TC)
      APE = INTGRL (0.0, PE)
      APC = INTGRL (0.0, PC)
      APD = INTGRL (0.0, PD)
      QIN = INTGRL (0.0, PEDVE)
      QOUT = INTGRL (0.0, PCDVC)
C     The following cards reset the old values and calculate the
      engine operating conditions.
      IF (KEEP.EQ.0) GO TO 20
      VEOLD = VE
      VCOLD = VC
      PEOLD = PE
      PCOLD = PC
      PDOLD = PD
      XTIME = TIME
      NUM = (N-1)*PSTEP
      IF(TIME.LE.NUM) GO TO 20
      AQIN(N) = QIN
      AQOUT(N) = QOUT
      AATE(N) = ATE
      AATC(N) = ATC
      AAPE(N) = APE
      AAPC(N) = APC
      AAPD(N) = APD
      IF(N.LE.M) GO TO 60
      AQINC = AQIN(N) - AQIN(N-M)
      AQOUTC = AQOUT(N) - AQOUT(N-M)
      AATEC = AATE(N) - AATE(N-M)
      AATCC = AATC(N) - AATC(N-M)
      AAPDC = AAPP(N) - AAPP(N-M)
      AAPCC = AAPC(N) - AAPC(N-M)
      AAPEC = AAPE(N) - AAPE(N-M)
      AVGTE = AATEC*FH
      AVGTC = AATCC*FH
      AVGPE = AAPEC*FH
      AVGPC = AAPCC*FH
      AVGPD = AAPDC*FH
      AVGPW = (AVGPE + AVGPC + AVGPD)/3.
      CF = PWAVG/AVGPW
      POIN = AQINC*FH*CF
      POUT = AQOUTC*FH*CF
      WOUT = POIN + POUT
      EFF = (AQINC + AQOUTC)/AQINC
```

```
60          CONTINUE
            N = N + 1
20          CONTINUE
C           The terminal segment inputs the integration method and the
            time step variable.  It also specifies the output variables.
TERMINAL
METHOD
PRINT       TE, TC, PE, PC, PD, ME, MC, MD, MW, VE, VC, VTOT, AVGTE,
            AVGTC, AVGPE, AVGPD, AVGPC, POIN, POUT, WOUT, EFF
C           The output cards print out the variables in graphical form.
OUTPUT      TE, TC
OUTPUT      PE, PC, PD
OUTPUT      ME, MC, MD, MW
OUTPUT      VE, VC, VTOT
TIMER       DELT =          ,FINTIM =         ,PRDEL =
END
STOP
```

A.2 Program B Listing (Common Pressure)

Program B (minus control cards)

```
TITLE RE-1000 ANALYSIS - AN IDEAL KINEMATIC MODE
TITLE PROGRAM B
C           The initial segment inputs the initial conditions and engine
            constants.
INITIAL
/           DIMENSION AQIN(500), AQOUT(500), AATE(500), ..., AATC(500),
            AAPWN(500)
            FIXED N,M
C           The following cards are input conditions for a given simula-
            tion.
INCON       THEAT = 900
INCON       TCOOL = 300
CONSTANT    KBC =          , NBC =
CONSTANT    HE =           , HC =
C           The following are engine parameters.
            XPMAX = 0.0210
            XDMAX = 0.0202
            AD = 0.002572
            AP = 0.002572
            AR = 0.000218
            VEAVG = 0.0000636
            VCAVG = 0.0001036
            VDH = 0.0000396
            VDR = 0.0000594
            VDC = 0.0000285
            DP = 0.05723
            DD = 0.05723
```

```
      FH = 30
      BDD = 45
      PWAVG = 7,000,000
      PB = 7,000,000
      ASEAVG = 0.01392
      ASCAVG = 0.02292
      Y14 = 0.667
      XDXP = 1.
      CP = 5200.
      R = 2080.
      PI = 3.1416.
C     The following cards calculate the engine parameters for all
      time t.
      CV = CP-R
      G = CP/CV
      GM1 = G-1.
      XPAMP = XPMAX*Y14
      XDAMP = XPAMP*XDXP
      TREG = (THEAT — TCOOL)/ALOG (THEAT/TCOOL)
      VDAVG = VDH + VDC + VDR
      TDAVG = VDAVG/(VDH/THEAT + VDR/TREG + VDC/TCOOL)
      FR = FH*2*PI
      B = BDD/180.*PI
C     The following cards calculate other engine parameters at
      time t = 0.
      VES = VEAVG — AD*SIN(B)
      VCS = VCAVG + (AD — AR)*SIN(B)
      MES = VEAVG*PWAVG/R/THEAT
      MCS = VCAVG*PWAVG/R/TCOOL
      MDS = VDAVG*PWAVG/R/TDAVG
      MWS = MES + MCS + MDS
      TE = THEAT
      TC = TCOOL
      ME = MES
      MC = MCS
      MD = MDS
      MW = MWS
      VEOLD = VES
      VCOLD = VCS
      MEOLD = MES
      MCOLD = MCS
      PWOLD = PW
C     The following cards are program control cards.
      XTIME = TIME
      AVGTE = 0.
      AVGTC = 0.
      AVGPWN = 0.
      POIN = 0.
      POUT = 0.
      WOUT = 0.
      EFF = 0.
      PSTEP =
```

```
            M =
            N = 1
C           The dynamic segment simulates the model.  The nosort card is
            required due to the FORTRAN logic programming.
DYNAMIC
NOSORT
C           The following cards make up the algebraic part of the
            formulation.
            TSTEP = TIME — XTIME
            XP = XDAMP*SIN (FR*TIME)
            XD = XDAMP*SIN (FR*TIME + B)
            VE = VEAVG — AD*XD
            VC = VCAVG + (AD — AR)*XD — AP*XP
            DVE = (VE — VEOLD)/TSTEP
            DVC = (VC — VCOLD)/TSTEP
            VTOT = VE + VC + VDAVG
            VRED = VE/TE + VC/TC + VDAVG/TDAVG
            ME = MW*VE/TE/VRED
            MC = MW*VC/TC/VRED
            MD = MW — ME — MC
            PW = MW*R/VRED
            PWN = (PW + PWOLD)/2.
            PWDVE = PWN*PVE
            PWDVC = PWD*DVC
            DME = (ME — MEOLD)/TSTEP
            DMC = (MC — MCOLD)/TSTEP
C           The following cards are the differential equations part of
            the formulation.
            DMW = (PB — PW)*KBC*(ABS (PB — PW))**NBC/ABS (PB — PW)
            MW = INTGRL (MWS, DMW)
            FE = INSW (DME, 1, 0.)
            FC = INSW (DMC, 1, 0.)
            TFE = FE*TE + (1. — FE)*THEAT
            TFC = FC*TC + (1. — FC)*TCOOL
            A11 = DVE/VE
            A22 = DVC/VC
            C11 = VE/TE/VRED + TFE*G/TE*(1. — VE/TE/VRED)
            C12 = VC/VRED/TC**2*(TE — TFE*G)
            C21 = VE/VRED/TE**2*(TC — TFC*G)
            C22 = VC/TC/VRED + TFC * G/TC*(1 — VC/TC/VRED)
            ASE = ASEAVG
            ASC = ASCAVG
            F1TEE = —A11*(TFE*G*(VE/TE/VRED — 1.) + G*TE — VE/VRED) +
            A22*VC*(TE — TFE*G)/TC/VRED + HE*ASE*(THEAT — TE)/CV/ME +
            DMW*(G*TFE-TE)/MW
            F2TEE = —A11*VE*(G*TFC-TC)/TE/VRED + A22*(G*TFC*(1.-
            VC/TC/VRED) + VC/VRED-G*TC) + HC*ASC*(TCOOL-TC)/CV/MC + DMW*
            (G*TFC-TC)/MW)
            DET = C11*C22 — C12*C21
            V1 = (F1TEE*C22 — C12*F2TEE)/DET
            TE = INTGRL (THEAT, V1)
            V2 = (F2TEE*C11 — F1TEE*C21)/DET
            TC = INTGRL (TCOOL, V2)
```

```
C           The following cards integrate TE, TC, PWN, PWDVE, and PWDVC
            ATE = INTGRL (0.0, TE)
            ATC = INTGRL (0.0, TC)
            APWN = INTGRL (0.0, PWN)
            QIN = INTGRL (0.0, PWDVE)
            QOUT = INTGRL (0.0, PWDVC)
C           The following cards reset the old values and calculate the
            engine operating parmaters.
            IF(KEEP.EQ.0) GO TO 20
            VEOLD = VE
            VCOLD = VC
            MEOLD = ME
            MCOLD = MC
            PWOLD = PW
            NUM = (N-1)*PSTEP
            IF(TIME.LE.NUM) GO TO 20
            AQIN(N) = QIN
            AQOUT(N) = QOUT
            AATE(N) = ATE
            AATC(N) = ATC
            AAPWN(N) = APWN
            IF(N.LE.M) GO TO 60
            AQINC = AQIN(N) — AQIN(N-M)
            AQOUTC = AQOUT(N) — AQOUT(N-M)
            AATEC = AATE(N) — AATE(N-M)
            AATCC = AATC(N) — AATC(N-M)
            AAPWNC = AAPWN(N) — AAPWN(N-M)
            AVGTE = AATEC*FH
            AVGTC = AATCC*FH
            AVGPWN = AAPWNC*FH
            CF = PWAVG/AVGPWN
            POIN = AQINC*FH*CF
            POUT = AQOUTC*FH*CF
            WOUT = POUT + POIN
            EFF = (AQINC + AQOUTC)/AQINC
60          CONTINUE
            N = N + 1
20          CONTINUE
C           The terminal section inputs the integration method and the
            time step variable.  Also the output variables are speci-
            fied.
TERMINAL
METHOD
PRINT       TE, TC, PW, ME, MC, MD, MW, VE, VC, VTOT, AVGTE, AVGTC,
            AVGPWN, POUT, POIN, WOUT, EFF
C           The output cards print out the variables in graphical form.
OUTPUT      TE, TC
OUTPUT      ME, MC, MD
OUTPUT      VE, VC, VTOT
OUTPUT      PW, MW
TIMER       DELT =          ,FINTIM =          ,PRDEL =
END
STOP
```

Reference

1. F. H. Speckpart and W. L. Green, *A Guide to Using CSMP — The Continuous System Modeling Program*, Prentice Hall, Inc., Englewood Cliffs, N.J., 1976.

Appendix B

VARIABLE LISTING

The following variables are defined in the model and in the programs. The FORTRAN form of the variables is shown in parentheses. The units of each variable are also given after the definition.

I. Thermodynamic Quantities (Variable)

T_e(TE) expansion space temperature (K)

T_c(TC) compression space temperature (K)

P_e(PE) expansion space pressure (N/m^2)

P_c(PC) compression space pressure (N/m^2)

P_d(PD) dead space pressure (N/m^2)

P_w(PW) working space pressure (uniform pressure assumption) (N/m^2)

m_e(ME) expansion space mass (kg)

m_c(MC) compression space mass (kg)

m_d(MD) dead space mass (kg)

m_w(MW) working space mass (kg)

II. Thermodynamic Quantities (Average over a cycle)

$\overline{T}_e$(AVGTE) average expansion space temperature (K)

$\overline{T}_c$(AVGTC) average compression space temperature (K)

$\overline{T}_{we}$(AVGWE) average expansion space wall temperature (K)

$\overline{T}_{wc}$(AVGWC) average compression space wall temperature (K)

$\overline{P}_e$(AVGPE) average expansion space pressure (N/m^2)

$\overline{P}_c$(AVGPC) average compression space pressure (N/m^2)

$\overline{P}_d$(AVGPD) average dead space pressure (N/m^2)

$\overline{P}_w$(AVGPW) average working space pressure (N/m^2)

$\overline{V}_e$(VEAVG) average expansion space volume (m^3)

$\overline{V}_c$(VCAVG) average compression space volume (m^3)

III. Thermodynamic Quantities (Starting values)

P_{ws}(PWS) starting fluid pressure (N/m^2)

V_{es}(VES) starting expansion volume (m^3)

V_{cs}(VCS) starting compression volume (m^3)

m_{es}(MES) starting expansion mass (kg)

m_{cs}(MCS) starting compression mass (kg)

m_{ds}(MDS) starting dead mass (kg)

IV. Engine Specification (Geometry)

$\overline{V}_d$(VDAVG) dead volume (m^3)

V_{dr}(VDR) regenerator volume (m^3)

V_{dc}(VDC) cooler volume (m^3)

V_{dh}(VDH) heater volume (m^3)

A_p(AP) piston cross-sectional area (m^2)

A_d(AD) displace cross-sectional area (m^2)

A_r(AR) rod cross-sectional area (m^2)

D_p(DP) piston diameter (m)

D_d(DD) displacer diameter (m)

D_r(DR) rod diameter (m)

$\overline{A}_{se}$(ASEAVG) average expansion space surface area (m^2)

$\overline{A}_{sc}$(ASCAVG) average compression space surface area (m^2)

$\overline{X}_{pm}$(XPMAX) maximum piston amplitude (m)

$\overline{X}_{dm}$(XDMAX) maximum displacer amplitude (m)

V. Engine Specifications (Operating conditions)

B_d(BDD) displacer phase angle (deg)

B(B) displacer phase angle (rad)

f(FH) engine operating frequency (Hz)

ω(FR) engine operating frequency (rad/s)

$\overline{T}_d$(TDAVG) dead volume average temperature (K)

T_{heat}(THEAT) heater temperature (K)

T_{cool}(TCOOL) cooler temperature (K)

T_{reg}(TREG) regenerator temperature (K)

T_{we}(TWE) expansion space average wall temperature (K)

T_{wc}(TWC) compression space average wall temperature (K)

X_{damp}(XDAMP) prescribed displacer motion amplitude (m)

X_{pamp}(XPAMP) prescribed piston motion amplitude (m)

X_d/X_p (XDXP) prescribed motion ratio (X_{damp}/X_{pamp}) (-)

Y14(Y14) prescribed amplitude ratio (X_{pamp}/X_{pm}) (-)

VI. Working Gas Properties

c_p(CP)	specific heat at constant pressure (J/kg•K)
c_v(CV)	specific heat at constant volume (J/kg•K)
R(R)	gas constant (J/kg•K)
γ(G)	ratio of specific heats (-)
γ-1(GM1)	heats ratio of specific heats (-)

Loss Coefficient

h_e(HE)	expansion space heat transfer coefficient ($W/m^2 \cdot K$)
h_c(HC)	compression space heat transfer coefficient ($W/m^2 \cdot K$)
k_{de}(KDE)	pressure drop flow coefficient (dead space to expansion space) (kg/Pa•s)
n_{de}(NDE)	pressure drop exponent (dead space to expansion space) (-)
k_{dc}(KDC)	pressure drop flow coefficient (dead space to compression space) (kg/Pa•s)
n_{dc}(NDC)	pressure drop exponent (dead space to compression space) (-)
k_{bc}(KBC)	seal leakage flow coefficient (compression space to bounce space) (kg/Pa•s)
n_{bc}(NBC)	seal leakage exponent (compression space to bounce space) (-)

Miscellaneous (FORTRAN variables not mentioned previously)

DELT	time step for integration
F_e(FE)	enthalpy flux switch (expansion space) (-)
F_c(FC)	enthalpy flux switch (compression space) (-)
FINTIM	ending time for simulation
PRDEL	printout time step (timer card)
PSTEP	printout time step (program)
M	number of PSTEPS per cycle
N	storage variable
T_{fe}(TFE)	enthalpy flux temperature (expansion space)
T_{fc}(TFC)	enthalpy flux temperature (compression space)
NUM	counter for storage
V_{red}(VRED)	defined in Eq. (C.7)

Appendix C

DERIVATIONS

The following derivations are required for this report.

C.1 Derivation 1 ($\overline{T}_d$ Calculation)

For this calculation, the dead space will be divided into three spaces (cooler, regenerator, and heater). These spaces are shown in Fig. C.1. The following assumptions are made for these spaces:

1. Each space has a uniform pressure.
2. All three spaces are at a uniform pressure.
3. The gas mass is well distributed throughout the dead space.

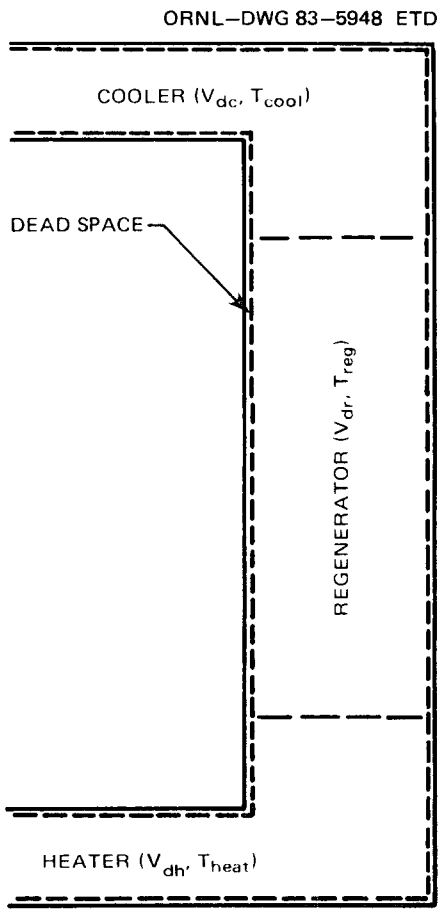

Fig. C.1. Division of dead space.

From the equation of state:

$$\overline{T}_d = \frac{P_d \ \overline{V}_d}{m_d \ R} \ .$$

Yet:

$$m_d = \frac{P_d \ V_{dr}}{R \ T_{reg}} + \frac{P_d \ V_{dc}}{R \ T_{cool}} + \frac{P_d \ V_{dh}}{R \ T_{heat}}$$

$$= \frac{P_d}{R} \left(\frac{V_{dr}}{T_{reg}} + \frac{V_{dc}}{T_{cool}} + \frac{V_{dh}}{T_{heat}} \right) \ .$$

Thus:

$$\overline{T}_d = \overline{V}_d \cdot \left(\frac{V_{dr}}{T_{reg}} + \frac{V_{dc}}{T_{cool}} + \frac{V_{dh}}{T_{heat}} \right)^{-1} \ ,$$

where the regenerator effective temperature is defined as:

$$T_{reg} = (T_{heat} - T_{cool})/\ln \ (T_{heat}/T_{cool}) \ .$$

C.2 Derivation 2 (Uniform Pressure Relations)

C.2.1 Algebraic relations for m_e, m_c, m_d, P_w

From conservation of mass:

$$m_w = m_e + m_c + m_d \ .$$

Substituting the perfect gas law (PV = MRT):

$$m_w = \frac{P_e \ V_e}{RT_e} + \frac{P_c \ V_c}{RT_c} + \frac{P_d \ \overline{V}_d}{R\overline{T}_d} \ .$$

Noting that $P_e = P_c = P_d = P_w$ (no pressure drop):

$$m_w = \frac{P_w}{R} \ \frac{V_e}{T_e} + \frac{V_c}{T_c} + \frac{\overline{V}_d}{\overline{T}_d} \ .$$

Solving for P_w:

$$P_w = \frac{m_w R}{\frac{V_e}{T_e} + \frac{V_c}{T_c} + \frac{\overline{V}_d}{\overline{T}_d}} . \tag{C.1}$$

Then, using Eq. (C.1) in the perfect gas law:

$$m_e = \frac{m_w V_e/T_e}{\frac{V_e}{T_e} + \frac{V_c}{T_c} + \frac{\overline{V}_d}{\overline{T}_d}} , \tag{C.2}$$

$$m_c = \frac{m_w V_c/T_c}{\frac{V_e}{T_e} + \frac{V_c}{T_c} + \frac{\overline{V}_d}{\overline{T}_d}} , \tag{C.3}$$

$$m_d = \frac{m_w \overline{V}_d/\overline{T}_d}{\frac{V_e}{T_e} + \frac{V_c}{T_c} + \frac{\overline{V}_d}{\overline{T}_d}} . \tag{C.4}$$

C.2.2 Differential relations for T_e, T_c

The expansion space will first be considered. The energy equation for this space is:

$$\frac{dT_e}{dt} = \frac{-T_e}{m_e}\frac{dm_e}{dt} - \frac{(\gamma - 1)\ T_e}{V_e}\frac{dV_e}{dt} + \frac{\gamma}{m_e}\frac{dm_e}{dt} \cdot T_{fe} + \frac{h_e \overline{A}_{se}}{m_e c_v}(T_{we} - T_e) . \tag{C.5}$$

The only unknown derivative in the above equation is dm_e/dt. This can be found by differentiating Eq. (C.2) with respect to time. Thus,

$$\frac{dm_e}{dt} = \frac{d}{dt}\left[\frac{m_w\ (V_e/T_e)}{\frac{V_e}{T_e} + \frac{V_c}{T_c} + \frac{\overline{V}_d}{\overline{T}_d}}\right] , \tag{C.6}$$

with

$$V_{red} = \frac{V_e}{T_e} + \frac{V_c}{T_c} + \frac{\overline{V}_d}{\overline{T}_d} \; . \tag{C.7}$$

Equation (C.6) reduces to:

$$\frac{dm_e}{dt} = m_e \left\{ \frac{1}{V_e}\frac{dV_e}{dt} - \frac{1}{T_e}\frac{dT_e}{dt} + \frac{1}{m_w}\frac{dm_w}{dt} - \frac{1}{V_{red}} \right.$$
$$\left. \times \left[\frac{V_e}{T_e}\left(\frac{1}{V_e}\frac{dV_e}{dt} - \frac{1}{T_e}\frac{dT_e}{dt}\right) + \frac{V_c}{T_c}\left(\frac{1}{V_c}\frac{dV_c}{dt} - \frac{1}{T_c}\frac{dT_c}{dt}\right) \right] \right\} \tag{C.8}$$

Substituting Eq. (C.8) into Eq. (C.5) and simplifying results in:

$$\frac{dT_e}{dt}\left[1 + (T_e - \gamma T_{fe})\left(-\frac{1}{T_e} + \frac{V_e}{V_{red}}\frac{1}{T_e^2}\right)\right] + \frac{dT_c}{dt}(T_e - \gamma T_{fe})$$
$$\times \left(\frac{V_c}{T_e^2\, V_{red}}\right) = \frac{1}{m_w}\frac{dm_w}{dt}(\gamma T_{fe} - T_e) + \frac{1}{V_e}\frac{dV_e}{dt}$$
$$\times \left[-(\gamma - 1)\, T_e - (T_e - \gamma T_{fe})\left(1 - \frac{V_e}{T_e\, V_{red}}\right)\right] + \frac{1}{V_c}\frac{dV_c}{dt}$$
$$\times (T_e - \gamma T_{fe})\left(\frac{V_c}{T_c\, V_{red}}\right) + \frac{h_e \overline{A}_{se}}{c_v m_e}(\overline{T}_{we} - T_e) \; .$$

A similar analysis can be done on the compression space energy equation. Here, the result of differentiating Eq. (C.3) is:

$$\frac{dm_c}{dt} = m_c \left\{ \left(\frac{1}{V_c}\frac{dV_c}{dt} - \frac{1}{T_c}\frac{dT_c}{dt} + \frac{1}{m_w}\frac{dm_w}{dt}\right) \right.$$
$$\left. - \frac{1}{V_{red}}\left[\frac{V_e}{T_e}\left(\frac{1}{V_e}\frac{dV_e}{dt} - \frac{1}{T_e}\frac{dT_e}{dt}\right) + \frac{V_c}{T_c}\left(\frac{1}{V_c}\frac{dV_c}{dt} - \frac{1}{T_c}\frac{dT_c}{dt}\right)\right] \right\} \; .$$

Thus, the energy equation for the compression space becomes:

$$\frac{dT_e}{dt}(T_c - \gamma T_{fc})\left(\frac{V_e}{T_e^2\ V_{red}}\right) + \frac{dT_c}{dt}\left[1 + (T_c - \gamma T_{fc})\left(\frac{-1}{T_c} + \frac{V_c}{T_c^2\ V_{red}}\right)\right]$$

$$= \frac{1}{m_w}\frac{dm_w}{dt}(\gamma T_{fc} - T_c) + \frac{1}{V_e}\frac{dV_e}{dt}(T_c - \gamma T_{fc})\left(\frac{V_e}{T_e\ V_{red}}\right)$$

$$+ \frac{1}{V_c}\frac{dV_c}{dt}\left[-(\gamma - 1)\ T_c - (T_c - \gamma T_{fc})\right.$$

$$\left.\times\left(1 - \frac{V_c}{T_c\ V_{red}}\right)\right] + \frac{h_c\bar{A}_{sc}}{c_v m_c}(\bar{T}_{wc} - T_c)\ .$$

Thus, in matrix form

$$\begin{bmatrix} C_{11} & C_{12} \\ C_{21} & C_{22} \end{bmatrix} \begin{bmatrix} \frac{dT_e}{dt} \\ \frac{dT_c}{dt} \end{bmatrix} = \begin{bmatrix} F_1 \\ F_2 \end{bmatrix}, \tag{C.9}$$

where

$$C_{11} = 1 + (T_e - \gamma T_{fe})\left(-\frac{1}{T_e} + \frac{V_e}{V_{red}\ T_e^2}\right),$$

$$C_{12} = (T_e - \gamma T_{fe})\frac{V_c}{T_c^2\ V_{red}},$$

$$C_{21} = (T_c - \gamma T_{fc})\frac{V_e}{T_e^2\ V_{red}},$$

$$C_{22} = 1 + (T_c - \gamma T_{fc})\left(-\frac{1}{T_c} + \frac{V_c}{T_c^2\ V_{red}}\right),$$

$$F_1 = -\left[(\gamma - 1)\, T_e + (T_e - \gamma T_{fe})\left(1 - \frac{V_e}{T_e\, V_{red}}\right)\right] \frac{1}{V_e}\frac{dV_e}{dt}$$

$$+ (T_e - \gamma T_{fe})\frac{V_c}{T_c\, V_{red}}\frac{1}{V_c}\frac{dV_c}{dt} + \frac{dm_w}{dt}\frac{1}{m_w}(\gamma T_{fe} - T_e)$$

$$+ \frac{h_e \bar{A}_{se}}{c_v m_e}(\bar{T}_{we} - T_e) \;,$$

$$F_2 = (T_c - \gamma T_{fc})\frac{V_e}{T_e\, V_{red}}\frac{1}{V_e}\frac{dV_e}{dt} + \frac{dm_w}{dt}\frac{1}{m_w}(\gamma T_{fc} - T_c)$$

$$- \left[(\gamma - 1)\, T_c + (T_c - \gamma T_{fc})\left(1 - \frac{V_c}{T_c\, V_{red}}\right)\right] \frac{1}{V_c}\frac{dV_c}{dt}$$

$$+ \frac{h_c \bar{A}_{sc}}{c_v m_c}(\bar{T}_{wc} - T_c) \;.$$

Appendix D

RESULTS (TABULAR FORM)

The actual numbers calculated by the CSMP program for all graphs are included for verification and possible further analysis by the reader. For each set of data, the compression and expansion space temperatures are also included with the engine performance calculations. The graph that portrays each table is also included.

Table D.1. Adiabatic cylinders

[Fig. 3(*a*) and (*b*)]

Y14	CR	$\overline{T}_e$ (K)	$\overline{T}_c$ (K)	W_{out} (W)	Efficiency (%)
0	0	900	300		66.67
0.2	1.13	873.9	305.0	441	64.58
0.4	1.28	847.6	310.1	1690	62.60
0.6	1.45	821.9	314.6	3611	60.37
0.8	1.66	796.7	318.2	6076	58.03
1.0	1.89	772.5	320.3	8906	55.47

Table D.2. Isothermal cylinders

[Fig. 3(*a*) and (*b*)]

Y14	$\overline{T}_e$ (K)	$\overline{T}_c$ (K)	W_{out} (W)	Efficiency (%)
0	900	300	0	66.67
0.2	900	300		66.67
0.4	900	300	1377	66.67
0.6	900	300	3120	66.67
0.8	900	300	5599	66.67
1.0	900	300	8853	66.67

Table D.3. Semi-adiabatic cylinder

[Fig. 5(*a*) and (*b*)]

h (W/m^2•K)	$\overline{T}_e$ (K)	$\overline{T}_c$ (K)	W_{out} (W)	Efficiency (%)
0	851.5	311.2	2496	63.01
10,000	885.5	302.2	2244	59.31
25,000	891.9	301.0	1991	56.73
62,500	896.4	300.5	1840	57.63
125,000	898.1	300.2	1875	60.88
∞	900.0	300.0	2031	66.67

Table D.4. Adiabatic cylinder-linear correlation

[Fig. 7(*a*) and (*b*)]

$1/k_{de}$, $1/k_{dc}$ (kg/Pa•s)$^{-1}$	$\overline{T}_e$ (K)	$\overline{T}_c$ (K)	W_{out} (W)	Efficiency (%)
0	851.5	311.2	2496	63.01
3.33×10^6	856.7	312.4	1942	54.11
6.67×10^6	861.3	314.0	1393	43.44
1×10^7	866.0	315.3	848	30.02
1.33×10^7	870.7	316.7	306	12.59

Table D.5. Isothermal cylinder-linear correlation

[Fig. 7(*a*) and (*b*)]

$1/k_{de}$, $1/k_{dc}$ (kg/Pa•s)$^{-1}$	$\overline{T}_e$ (K)	$\overline{T}_c$ (K)	W_{out} (W)	Efficiency (%)
0	900	300	2031	66.67
3.33×10^6	900	300	1529	57.10
6.67×10^6	900	300	1009	44.27
1×10^7	900	300	487	26.09
1.25×10^7	900	300	99.1	6.38

Table D.6. Adiabatic cylinder-nonlinear correlation

[Fig. 9(*a*) and (*b*)]

$1/k_{de}$, $1/k_{dc}$ $(kg/s \cdot Pa^{0.57})^{-1}$	$\overline{T}_e$ (K)	$\overline{T}_c$ (K)	W_{out} (W)	Efficiency (%)
0	851.5	311.2	2496	63.01
13,333	867.3	311.2	2322	60.24
20,000	859.6	311.8	2137	57.18
30,000	858.8	312.9	1751	50.24
40,000	862.2	314.3	1263	39.98
50,000	867.0	315.8	685	24.82

Table D.7. Isothermal cylinder-nonlinear correlation

[Fig. 9(*a*) and (*b*)]

$1/k_{de}$, $1/k_{dc}$ $(kg/s \cdot Pa^{0.57})^{-1}$	$\overline{T}_e$ (K)	$\overline{T}_c$ (K)	W_{out} (W)	Efficiency (%)
0	900	300	2031	66.67
13,333	900	300	1844	63.27
20,000	900	300	1713	60.69
30,000	900	300	1382	53.59
40,000	900	300	948	42.18
50,000	900	300	437	23.70

Table D.8. Adiabatic cylinder-linear correlation

[Fig. 10(*a*) and (*b*)]

k_{bc} (kg/Pa•s)	$\overline{T}_e$ (K)	$\overline{T}_c$ (K)	W_{out} (W)	Efficiency (%)
0	851.5	311.2	2496	63.01
0.5×10^{-8}	851.9	311.7	2060	54.29
1×10^{-8}	853.6	312.8	1605	45.23
2×10^{-8}	859.2	313.3	759	25.93
3×10^{-8}	866.3	312.6	111	4.82

Table D.9. Isothermal cylinder-linear correlation

[Fig. 10(*a*) and (*b*)]

k_{bc} (kg/Pa•s)	$\overline{T}_e$ (K)	$\overline{T}_c$ (K)	W_{out} (W)	Efficiency (%)
0	900	900	2031	66.67
0.5×10^{-8}	900	900	1810	60.53
1×10^{-8}	900	900	1562	54.15
2×10^{-8}	900	900	1054	40.78
3×10^{-8}	900	900	590	26.55

Table D.10. Adiabatic cylinder-nonlinear correlation

[Fig. 12(*a*) and (*b*)]

k_{bc} (kg/s•Pa$^{0.57}$)	$\overline{T}_e$ (K)	$\overline{T}_c$ (W)	W_{out} (W)	Efficiency (%)
0	851.5	311.2	2496	63.01
2.5×10^{-6}	852.3	312.1	1896	51.01
5×10^{-6}	855.4	313.3	1257	37.91
7.5×10^{-6}	860.2	313.2	659	23.24
10×10^{-6}	866.0	312.5	149	6.43
12.5×10^{-6}	872.1	311.4	−243	−13.23

Table D.11. Isothermal cylinder-nonlinear correlation

[Fig. 12(*a*) and (*b*)]

k_{bc} (kg/s•Pa$^{0.57}$)	T_e (K)	T_c (K)	W_{out} (W)	Efficiency (%)
0	900	300	2031	66.67
2.5×10^{-6}	900	300	1680	57.19
5.0×10^{-6}	900	300	1283	47.00
7.5×10^{-6}	900	300	880	35.88
10.0×10^{-6}	900	300	503	23.54
12.5×10^{-6}	900	300	173	9.60

Table D.12. Case 1 — Adiabatic cylinders

(Table 1, Case 1)

k_{bc} (kg/Pa•s)	$1/k_{de}$, $1/k_{dc}$ $(kg/Pa\cdot s)^{-1}$	$\overline{T}_e$ (K)	$\overline{T}_c$ (K)	W_{out} (W)	Efficiency (%)
0	0	851.5	311.2	2496	63.01
1×10^{-8}	0	853.6	312.8	1605	45.23
0	6.6×10^{6}	861.3	314.0	1393	43.44
1×10^{-8}	6.6×10^{6}	863.7	315.5	562	20.03

Table D.13. Case 2 — Isothermal cylinders

(Table 1, Case 2)

k_{bc} (kg/Pa•s)	$1/k_{de}$, $1/k_{dc}$ $(kg/Pa\cdot s)^{-1}$	$\overline{T}_e$ (K)	$\overline{T}_c$ (K)	W_{out} (W)	Efficiency (%)
0	0	900	300	2031	66.67
1×10^{-8}	0	900	300	1562	54.14
0	6.6×10^{6}	900	300	1010	44.29
1×10^{-8}	6.6×10^{6}	900	300	565	26.47

Table D.14. Semi-adiabatic cylinders

(Table 1, Case 3)

k_{bc} (kg/Pa•s)	$1/k_{de}$, $1/k_{dc}$ $(kg/Pa\cdot s)^{-1}$	$\overline{T}_e$ (K)	$\overline{T}_c$ (K)	W_{out} (W)	Efficiency (%)
0	∞	896.4	300.5	1840	57.63
1×10^{-8}	∞	896.7	300.6	1242	43.31
0	6.6×10^{6}	897.2	300.6	816	33.27
1×10^{-8}	6.6×10^{6}	897.4	300.8	268	12.52

Appendix E

RE-1000 DATA

Table E.1. Description of geometry for RE-1000 free-piston Stirling engine

Number of cylinders	1
Type	Free piston with dashpot
Working fluid	Helium
Design frequency, Hz	30
Design pressure, MPa	7.0
Design power, W	1000
Design phase angle, deg	45
Cylinder bore, cm (in.)	5.723 (2.2527)
Maximum displacer stroke, cm (in.)	4.04 (1.591)
Maximum power piston stroke, cm (in.)	4.20 (1.654)
Cooler	
Description	135 rectangular passages
Passage width, cm (in.)	0.0508 (0.020)
Passage depth, cm (in.)	0.376 (0.148)
Length, cm (in.)	7.92 (3.118)
Flow area, cm^2 ($in.^2$)	2.58 (0.400)
Wetted perimeter, cm (in.)	115.2 (45.354)
Volume, cm^3 ($in.^3$)	20.42 (1.246)
Heater	7181 tubes
Description	Tubular
Tube length, cm (in.)	18.34 (7.220)
Tube inside diameter, mm (in.)	2.362 (0.093)
Tube outside diameter, mm (in.)	3.175 (0.125)
Number of tubes	34
Design maximum wall temperature, °C (°F)	650 (1202)
Regenerator	
Length containing wire mesh, cm (in.)	6.446 (2.538)
Outside diameter, cm (in.)	7.18 (2.827)
Inside diameter, cm (in.)	6.07 (2.390)
MATRIX	304SS METEX
Wire diameter, μm (in.)	88.9 (0.0035)
Porosity, %	75.9
Weight, g (lb)	139 (0.31)
Pistons	
Power piston mass, kg (lb)	6.2 (13.67
Displacer mass, kg (lb)	0.426 (0.94)
Piston diameter, cm (in.)	5.718 (2.2514)
Displacer diameter, cm (in.)	5.67 (2.232)
Displacer rod diameter, cm (in.)	1.663 (0.655)
Piston length, cm (in.)	28.0 (11.024)
Displacer length, cm (in.)	15.19 (5.980)

Table E.1 (continued)

Dead volumes	
Expansion space to heater tube junction, cm^3 ($in.^3$)	3.80 (0.23)
Heater tube to regenerator plenum junction, cm^3 ($in.^3$)	5.90 (0.36)
Regenerator plenum at hot end of regenerator, cm^3 ($in.^3$)	4.10 (0.25)
Regenerator plenum ring, cm^3 ($in.^3$)	0.83 (0.05)
Displacer/cylinder annular ring, cm^3 ($in.^3$)	10.06 (0.61)
Auxiliary instrument port (hot), cm^3 ($in.^3$)	1.56 (0.10)
Regenerator plenum at cold end of regenerator, cm^3 ($in.^3$)	4.23 (0.26)
Regenerator plenum ring, cm^3 ($in.^3$)	0.83 (0.05)
Cooler plenum at compression space, cm^3 ($in.^3$)	7.15 (0.44)
Cylinder ports, cm^3 ($in.^3$)	1.21 (0.07)
Heater flange fittings, cm^3 ($in.^3$)	3.41 (0.21)
Piston/spider clearance, cm^3 ($in.^3$)	38.7 (2.36)
Annular ring around spider, cm^3 ($in.^3$)	3.82 (0.23)
DCDT core, cm^3 ($in.^3$)	0.79 (0.05)
Gas spring midport hardware, cm^3 ($in.^3$)	8.31 (0.51)
Auxiliary instrument ports (regen/cooler), cm^3 ($in.^3$)	0.93 (0.06)
Auxiliary instrument ports (compression), cm^3 ($in.^3$)	3.15 (0.19)
Cooler, cm^3 ($in.^3$)	20.42 (1.23)
Regenerator, cm^3 ($in.^3$)	49.42 (3.02)
Heater, cm^3 ($in.^3$)	26.50 (1.62)
Materials	
Heater head	
Regenerator outer cylinder	316SS
Expansion space dome	316SS
Regenerator inner wall cylinder	304SS
Displacer	321SS
Cooler	6061-T6 Al
Cylinder	
Power piston	6061-T6 Al with chrome oxide coating
Displacer	304SS with chrome oxide coating
Piston body	6061-T6 Al with chrome oxide coating
Design Clearances (diam)	
Displacer rod/rod cylinder, μm (in.)	25.4 (0.0010)
Displacer body/displacer cylinder, μm (in.)	381.0 (0.015)
Power piston/piston cylinder, μm (in.)	33.0 (0.0013)
Displacer gas spring	
Design mean volume, cm^3 (in^3)	31.79 (1.94)
Piston diameter, cm (in.)	1.633 (0.65)

Source: J. Schreiber, *Testing and Performance Characteristic of a 1-kW Free-Piston Stirling Engine*, NASA Technical Memorandum 82999, 1983.

Internal Distribution

1. R. D. Banduric
2. F. Chen
3-7. N. C. J. Chen
8. F. A. Creswick
9. J. L. Crowley
10. N. Domingo
11. R. D. Ellison
12. P. D. Fairchild
13. W. Fulkerson
14. F. P. Griffin
15. D. S. Griffith
16. V. O. Haynes
17. W. L. Jackson
18. R. E. MacPherson
19. J. W. Michel
20. R. E. Minturn
21. G. T. Privon
22. J. P. Sanders
23. H. E. Trammell
24. C. D. West
25. ORNL Patent Office
26. Central Research Library
27. Document Reference Section
28-29. Laboratory Records Department
30. Laboratory Records (RC)

External Distribution

31. R. J. Fiskum, Program Manager, Energy Conversion Equipment Branch, CE 113.2, Rm. GH068, Department of Energy, 1000 Independence Avenue, S.W., Washington, DC 20585
32. J. D. Ryan, Acting Chief, Energy Conversion Equipment Branch, CE 113.2, Rm. GH068, Department of Energy, 1000 Independence Ave. S.W., Washington, DC 20585
33. Office of Assistant Manager for Energy Research and Development, Department of Energy, ORO, Oak Ridge, TN 37831
34-60. Technical Information Center, Department of Energy, Oak Ridge, TN 37831